Saku Siermala

Zero-sequence current injection theory and injection-based coil tuning in compensated distribution networks

School of Technology and Innovation
Master's thesis in Electrical Engineering
Energy and Information Technology, M.Sc. (Tech.)

Vaasa 2023

UNIVERSITY OF VAASA
Tekniikan ja innovaatiojohtamisen yksikkö
Author: Saku Siermala
Title of the thesis: Zero-sequence current injection theory and injection-based coil tuning in compensated distribution networks
Degree: Master of Science in Technology
Programme: Electrical Engineering
Supervisor: Kimmo Kauhaniemi
Instructor: Anna Kulmala
Evaluator: Mazaher Karimi
Year: 2023 **Pages:** 101

ABSTRACT :

This thesis aims to derive and document zero-sequence current injection theory in compensated distribution networks. More specifically, the objective is to derive a comprehensive set of equivalent circuits and equations that describe the primary interactions between the current injection and system parameters. The auxiliary zero-sequence current injection is an essential method addressing various complex applications in compensated networks, including tuning arc suppression coil, detecting high impedance faults, locating earth faults, and residual earth fault currents compensation. This thesis explicitly considers the current injection when current is injected into the zero-sequence system through the network's neutral point via the power auxiliary winding of the arc suppression coil.

The theoretical part of the thesis introduces the fundamentals of compensated networks, including system damping, detuning, unbalance, and their influence on the natural zero-sequence voltage. Regarding the current injection, the idea, implementation, and key applications of the concept are presented, including the derivation of injection theory that describes the phenomenon. The injection theory defines the impact of current injection on a compensated network by deriving relevant equations and equivalent circuits that describe the system's response to the injection and the parameters affecting it. The injection theory is also verified and visualized using PSCAD and MATLAB software.

Additionally, the thesis includes a literature review on commercial injection-based coil tuning solutions. Current injection is an attractive method for arc suppression coil tuning, enabling operation in fully symmetrical networks and faster tuning without additional coil movements. The scope of the review focuses on the following well-known products: current injection device ECI by Trench Group, Current Injection for Low or Highly Variable Zero-Sequence Voltages by A. Eberle Gmbh & Co.KG, and Multi-Frequency Current Injection by A. Eberle Gmbh & Co.KG and EGE spol. s r.o. The review aims to describe the design and functionality of the previous products and highlight the key differences and advantages of the different solutions. The source material of the review includes product data sheets, scientific publications, and related patents.

In total, the result of the thesis is an extensive collection of current injection theory, including equations, graphs, and equivalent circuits describing the phenomenon. Moreover, the thesis provides a comprehensive literature review on commercial injection-based coil tuning solutions.

KEYWORDS: current injection, arc suppression coil, multi-frequency current injection, compensated distribution networks, earth fault current compensation

VAASAN YLIOPISTO
Tekniikan ja innovaatiojohtamisen yksikkö
Tekijä: Saku Siermala
Tutkielman nimi: Zero-sequence current injection theory and injection-based coil tuning in compensated distribution networks
Tutkinto: Diplomi-insinööri
Oppiaine: Sähkötekniikka
Työn valvoja: Kimmo Kauhaniemi
Työn ohjaaja: Anna Kulmala
Työn tarkastaja: Mazaher Karimi
Valmistumisvuosi: 2023 **Sivumäärä:** 101

TIIVISTELMÄ:

Tämän diplomityön tavoitteena on virtainjektioteorian selvittäminen, johtaminen ja dokumentointi kompensoiduissa sähkönjakeluverkoissa. Erityisesti työn tavoitteena on tuottaa kattavat virtainjektiota kuvaavat sijaiskytkennät ja yhtälöt, jotka määrittelevät pääasiallisia vuorovaikutuksia injektion ja verkon järjestelmäparametrien välillä. Virtainjektio on olennainen menetelmä, jota sovelletaan moniin haastaviin sovelluksiin kompensoiduissa verkoissa, kuten kompensointikelan viritys, suuri-impedanssisten vikojen havainnointi, maasulun paikantaminen ja jäännösmaasulkuvirran kompensointi. Tässä työssä virtainjektiota käsitellään erityisesti, kun virtaa syötetään järjestelmän nollajärjestelmään kompensointikelan tehoapukäämin kautta.

Työn teoriaosuudessa käsitellään kompensoitujen verkkojen perusteoriaa, mukaan lukien järjestelmän vaimennusta, vinoviritystä ja epäsymmetriaa sekä niiden vaikutus verkon luonnolliseen nollajännitteeseen. Virtainjektion osalta esitetään konseptin idea, toteutus ja keskeiset sovellukset sekä johdetaan ilmiötä kuvaava virtainjektioteoria. Virtainjektioteoria määrittää injektion aiheuttaman vaikutuksen verkkoon, sisältäen johdetut yhtälöt ja sijaiskytkennät, jotka kuvaavat järjestelmän vasteen injektioon ja tuovat esiin siihen vaikuttavat parametrit. Johdettu injektioteoria verifioidaan ja visualisoidaan hyödyntäen PSCAD ja MATLAB ohjelmistoja.

Lisäksi työ sisältää kirjallisuuskatsauksen kaupallisiin virtainjektioperusteisiin kompensointikelan säätömenetelmiin. Virtainjektion käyttö kelan säädössä onkin suosittu menetelmä, koska se mahdollistaan toiminnan täysin symmetrisissä verkoissa ja nopeamman virityksen ilman ylimääräisiä kelan liikkeitä. Tarkemmin katsauksessa keskitytään seuraaviin tunnettujen valmitajien tuotteisiin: Trench Group:n virtainjektori ECI, A. Eberle Gmbh & Co.KG:n virtainjektiolaitteisto pienille tai erittäin vaihteleville nollajännitteille, A. Eberle Gmbh ja Co.KG:n and EGE spol. s r.o:n yhdessä kehittämä monitaajuusvirtainjektiolaite. Katsauksen tavoite on kuvata tuotteiden toimintaa ja toimivuutta sekä tuoda esiin eri ratkaisujen keskeiset erot ja edut. Lähdeaineistona käytetään tuotteiden datalehtiä, tieteellisiä julkaisuja ja aiheeseen liittyviä patentteja.

Kokonaisuudessaan diplomityön lopputuloksena on laaja kokoelma virtainjektioteoriaa, sisältäen ilmiötä kuvaavia yhtälöitä, kuvaajia sekä sijaiskytkentöjä. Lisäksi opinnäytetyö tarjoaa kattavan kirjallisuuskatsauksen kaupallisista injektioperusteisista kelan säätöratkaisuista.

AVAINSANAT: virtainjektio, kompensointikela, monitaajuusvirtainjektio, kompensoidut sähkönjakeluverkot, maasulkuvirran kompensointi

Contents

Figures

Tables

Table 5. Equations that describe the system at fundamental frequency during voltage source-based non-fundamental frequency injection. 57

Symbols and Abbreviations

Greek symbols

ΔB_s	system detuning in terms of susceptance at the fundamental frequency of the system
ω_1	angular frequency at frequency f_1 unequal to frequency f_2
ω_2	angular frequency at frequency f_2 unequal to frequency f_1
ω_i	angular frequency at frequency f_i that is complementary frequency to frequency f_{ii}
ω_{ii}	angular frequency at frequency f_{ii} that is complementary frequency to frequency f_i
ω_n	angular frequency at frequency f_n
ω_{res}	angular frequency at the resonant frequency f_{res}
ω_s	synchronous angular frequency, i.e., the angular frequency at the fundamental frequency of the system

Other symbols

$\bar{a}$	phase shift operator
B_A	phase-to-ground susceptance of phase A
B_{cNet}	capacitive phase-to-ground susceptance of the network
B_{Coil}	inductive susceptance of the central coil
$B_{CoilNet}$	inductive susceptance of the distributed coils
$B_{CoilTot}$	inductive susceptance of all connected arc suppression coils, including distributed compensation

B_{EFNet}	capacitive susceptance of the network seen by the central compensation, i.e., uncompensated capacitive susceptance of the network by the distributed compensation
B_{inj_f1}	zero-sequence susceptance of the system at frequency f_1
B_{inj_f2}	zero-sequence susceptance of the system at frequency f_2
B_{inj_fi}	zero-sequence susceptance of the system at frequency f_i
B_{inj_fii}	zero-sequence susceptance of the system at frequency f_{ii}
B_{inj_fn}	zero-sequence susceptance of the system at frequency f_n
C_A	phase-to-ground capacitance of phase A
C_{EFNet}	phase-to-ground capacitance of the network seen by the central compensation, i.e., uncompensated phase-to-ground capacitance of the network by the distributed compensation
C_{Net}	phase-to-ground capacitance of the network
$d\overline{I}_{in}$	differential of injected current
$d\overline{U}_0$	differential of zero-sequence voltage
$\overline{E}_A$	operating voltage of the phase A
$\overline{E}_B$	operating voltage of the phase B
$\overline{E}_C$	operating voltage of the phase C
f_1	non-fundamental frequency that is unequal to frequency f_2
f_2	non-fundamental frequency that is unequal to frequency f_1
f_{high}	approximated upper limit of the MCI's frequency range
f_i	non-fundamental frequency that is complementary frequency to frequency f_{ii}
f_{ii}	non-fundamental frequency that is complementary frequency to frequency f_i
f_{1ow}	approximated lower limit of the MCI's frequency range

f_n	frequency unequal to the fundamental frequency of the system
f_{res}	resonant frequency of the zero-sequence system
f_s	synchronous, i.e., fundamental or mains frequency of the system
G_{0Tot}	total phase-to-ground conductance of the system, including the parallel resistor and losses of the ASC
G_A	phase-to-ground conductance of the phase A
G_{Coil}	conductance of the parallel resistor
G_{Net}	phase-to-ground conductance, i.e., shunt losses, of the network
$\overline{I}_{0Tr}$	zero-sequence current of the earthing or main transformer
$\overline{I}_A$	line current of phase A
$\overline{I}_{asymm}$	asymmetrical line-to-ground current concentrated in phase A
$\overline{I}_B$	line current of phase B
$\overline{I}_C$	line current of phase C
$\overline{I}_{Coil}$	zero-sequence current measured at coil
I_{Coil}	inductive current produced by the central coil
$I_{CoilNet}$	inductive current produced by distributed compensation
$I_{CoilTot}$	inductive current produced by all the connected arc suppression coils, including distributed compensation
I_{cNet}	capacitive earth fault current of the network
I_d	system damping, i.e., the total shunt losses of the system in amperes
I_{EFNet}	capacitive earth fault current seen by the central compensation, i.e., uncompensated earth fault current of the network by the distributed compensation

$\overline{I}_{in}$	current produced by the injection device or the total current that flows through the injection device, depending on the presentation of the injection device
$\overline{I}_{in\_fn}$	current produced by the injection device at frequency f_n
$\overline{I}_{in\_fs}$	current that flows through the injection device at the fundamental frequency of the system f_s
I_v	system detuning in amperes
j	imaginary unit
K_{fn}	ratio between the zero-sequence voltage phasors measured at coil and busbar
L_{0Tr}	zero-sequence inductance of the earthing or main transformer through which the coil is connected to the network
L_{Coil}	inductance of the central arc suppression coil, including fixed central coils
$L_{CoilNet}$	inductance of the distributed coils
$L_{CoilTot}$	inductance of all connected arc suppression coils, including distributed compensation
R_A	phase-to-ground resistance of phase A
R_{par}	resistance of the parallel resistor
$\overline{U}_0$	zero-sequence voltage measured at busbar
$\overline{U}_{0\_fn}$	zero-sequence voltage measured at busbar at frequency f_n
$\overline{U}_{0\_fs}$	zero-sequence voltage measured at busbar at the fundamental frequency of the system f_s during injection
$\overline{U}_{0Coil}$	zero-sequence voltage measured at coil
$\overline{U}_{0Coil\_fn}$	zero-sequence voltage measured at coil at frequency f_n
$\overline{U}_{0Coil\_fs}$	zero-sequence voltage measured at coil at the fundamental frequency of the system f_s during injection

$\overline{U}_{0Tr}$	zero-sequence voltage over the earthing or main transformer
$\overline{U}_A$	phase-to-ground voltage of phase A
$\overline{U}_B$	phase-to-ground voltage of phase B
$\overline{U}_C$	phase-to-ground voltage of phase C
$\overline{U}_{in}$	source voltage of voltage source-based injection
$\overline{U}_{in\_fn}$	source voltage of voltage source-based injection at frequency f_n
U_{PE}	rated positive sequence phase-to-ground voltage
$\overline{Y}_{0Tr}$	zero-sequence admittance per phase of the earthing or main transformer through which the coil is connected to the network. For the single-phase presentation, a coefficient of three is applied.
$\overline{Y}_A$	phase-to-ground admittance of phase A
$\overline{Y}_{asymm}$	asymmetrical phase-to-ground admittance concentrated in phase A
$\overline{Y}_B$	phase-to-ground admittance of phase B
$\overline{Y}_C$	phase-to-ground admittance of phase C
$\overline{Y}_{Coil}$	admittance of the arc suppression coil, including the conductance of the parallel resistor
$\overline{Y}_{in}$	source admittance of the injection device
$\overline{Y}_{inj}$	zero-sequence admittance seen from the terminals of the injection
$\overline{Y}_{inj\_f1}$	zero-sequence admittance of the system at frequency f_1
$\overline{Y}_{inj\_f2}$	zero-sequence admittance of the system at frequency f_2
$\overline{Y}_{inj\_fi}$	zero-sequence admittance of the system at frequency f_i
$\overline{Y}_{inj\_fii}$	zero-sequence admittance of the system at frequency f_{ii}

$\overline{Y}_{inj\_fn}$	zero-sequence admittance seen from the terminals of the injection at frequency f_n
$\overline{Y}_{Net}$	total phase-to-ground admittance of the network
$\overline{Y}_{symm}$	symmetrical phase-to-ground admittance. One-third per phase.
$\overline{Z}_{0Tr}$	zero-sequence impedance per phase of the earthing or main transformer through which the coil is connected to the network. For the single-phase presentation, one-third is applied.
Z_{0Tr}	magnitude of zero-sequence impedance of the earthing or main transformer
$\overline{Z}_{inj}$	zero-sequence impedance seen from the terminals of the injection
$\overline{Z}_{inj\_fn}$	zero-sequence impedance seen from the terminals of the injection at frequency f_n
$\overline{Z}_{inj\_fres}$	zero-sequence impedance seen from the terminals of the injection at the resonant frequency f_{res}

Abbreviations

ASC	Arc Suppression Coil, Petersen coil
CIF	Control by Injecting Frequencies
ECI	current injection device ECI
HIF	High Impedance Fault
HV	High Voltage
MATLAB	MATrix LABoratory
MCI	Multi-Frequency Current Injection
MV	Medium Voltage
NPDV	Neutral Point Displacement Voltage

NVD	Neutral Voltage Displacement
PAW	Power Auxiliary Winding
PSCAD	Power Systems Computer Aided Design
RCC	Residual Current Compensation
RMS	Root Mean Square

1 Introduction

In modern power systems, a reliable operation of distribution networks is essential for ensuring uninterrupted electricity supply. As a result of the large-scale cabling of distribution networks, the shunt capacitances, and thus also the earth fault currents, of the network have increased significantly. Compensated distribution networks, equipped with various technical implementations, aim to mitigate the adverse effects of earth faults and enhance the network's overall performance. In a compensated distribution network, the neutral point is earthed via an arc suppression coil (ASC), reducing the capacitive earth fault currents and dangerous hazard voltages at the fault location significantly, which has led to the worldwide popularity of compensated medium voltage distribution networks.

One rapidly developed technology in compensated distribution networks is the utilization of auxiliary signals that are increasingly applied in several applications. Current injection refers to an operation where an auxiliary current signal is supplied into the network, usually directly to the neutral point of the system via power auxiliary winding of the arc suppression coil, thus enabling a given application to monitor and evaluate the system's response. The auxiliary signal itself can be produced in several ways depending on the requirements of the application and the cost of the implementation.

This thesis is done in cooperation with ABB Oy Distribution Solutions. The main aim of the thesis is the derivation and documentation of injection theory, including the equivalent circuits and equations that describe the system's response to injection and the parameter affecting it. The derived injection theory is further verified and visualized using the PSCAD simulation environment and MATLAB software. In addition, the thesis includes a literature review on the injection-based tuning of ASC, which is a major application to which the current injection is applied.

Several well-established current injection-based coil tuning solutions are already available in the market. Traditionally, the injection current is supplied at the operating fundamental frequency of the system. However, today's most advanced current injection-based coil tuning solutions utilize multiple frequencies unequal to the fundamental frequency to calculate the position of ASC. In this thesis, especially, the following three commercial products are reviewed:

- The current injection device ECI by Trench Group operating under Siemens Energy AG
- Current Injection for Low or Highly Variable Zero-Sequence Voltages (CI) by A. Eberle Gmbh & Co.KG
- Multi-Frequency Current Injection (MCI) by A. Eberle Gmbh & Co.KG and EGE spol. s r.o.

Chapter 2 introduces the fundamentals of compensated distribution networks, including the technical aspects of earth fault compensation, while Chapter 3 covers the fundamentals of the neutral point voltage, including the resonance curve. The pivotal concept, implementation, and applications of current injection are introduced in Chapter 4, along with the comprehensive derivation of injection theory. Chapter 5 verifies the injection theory through PSCAD simulations. Finally, the commercial injection-based methods for arc suppression coil tuning are reviewed in Chapter 6.

2 Earth fault in a compensated distribution network

An earth fault is a common fault where a live part of the electric network comes into conductive contact with the ground. Earth fault can also include ground connection to two or three phases, in which case it is called a two- or three-phase earth fault, respectively. During the earth fault, a fault current is generated, which flows from the phase to earth either directly or via fault resistance.

2.1 Technical implementation of compensation

The neutral point of the compensated distribution network, also known as resonant earthed system or high impedance earthed system, is earthed via arc suppression coil (ASC), also known as Petersen coil after the inventor of the method. In practice, compensation is implemented as centralized, distributed, or a combination of both (Wahlroos et al., 2011, p. 3). In centralized compensation, the ASC can be connected to the neutral point of the earthing transformer at the substation. In addition, if there is a neutral point on the secondary side of the main transformer of the distribution network, the ASC can be connected to the main transformer. Distributed compensation is implemented by placing a fixed coil in one or more feeders (Wahlroos et al., 2011, p. 5).

2.1.1 Earthing transformer

In Finland, the windings of main transformers at 110/20 kV substations are usually YNd11 configured, in which case no neutral point is available to connect the ASC on the low voltage side (Mäkinen, p. 179). In this case, a ZN-configured earthing transformer can create an alternative neutral point. The connection of the earthing transformer to the compensated network is shown in Figure 1.

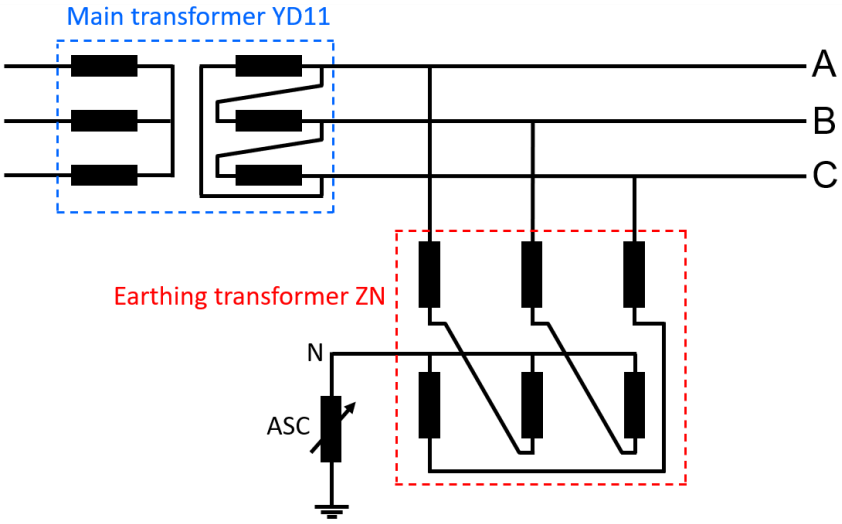

Figure 1. Connection of earthing transformer and arc suppression coil.

In many cases, the zero-sequence impedance of the earthing transformer is neglected because its effect is not significant. However, due to the grid sizes used today, the transformer zero-sequence impedance already reaches values of 10 to 20 % of the tuned arc suppression coil impedance (Druml & Kugi, 2005, p. 2–3). It, therefore, is no longer negligible for determining the correct coil position. Furthermore, it should be noted that the zero-sequence impedance is an inductive frequency-dependent component, and thus it is more significant at higher frequencies.

2.1.2 Parallel resistor

A parallel resistor, also known as an earthing resistor, is commonly connected to the zero-sequence system in the power auxiliary windings of the ASC. A parallel resistor is used during a fault to increase the resistive component of the earth fault current, improving the accuracy of the protection relays, especially when the fault resistance is low (Wahlroos et al., 2011, p. 4). The parallel resistor can also be permanently connected to limit the natural zero-sequence voltage of the network, which may be advantageous in rural networks where the natural zero-sequence voltage is high (Wahlroos et al., 2011, p. 4).

2.2 Earth fault current compensation

The uncompensated earth fault current consists of a capacitive and a resistive component. Since the neutral point of the compensated network is earthed via ASC, the inductive current produced by the coil during the earth fault is in the opposite phase to the capacitive earth fault current produced by the network (Lakervi & Partanen, 2009, pp. 184–185). Thus, the inductive component of the earth fault current produced by the ASC opposes the capacitive component produced by the capacitive shunt admittances of the feeders. However, the ASC cannot reduce the resistive component of the earth fault current but instead increases it with its own losses (Wahlroos et al., 2021, p. 8). The principle of earth fault current compensation is illustrated in Figure 2.

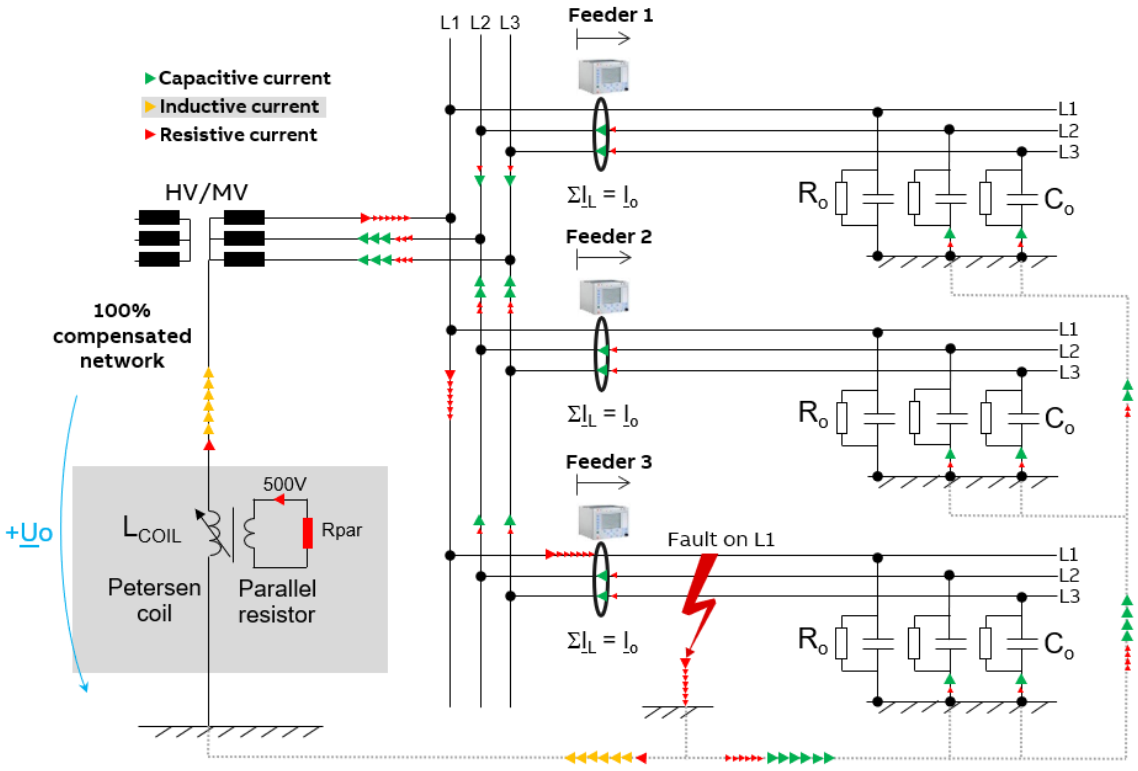

Figure 2. Earth fault in the compensated distribution network (adapted from Wahlroos, 2017).

2.3 Detuning degree

The term detuning degree, also known as compensation degree, refers to the ratio of inductive current produced by all the connected ASCs, including distributed compensation, to the capacitive current produced by the phase-to-ground admittances of the feeders of the whole network (Wahlroos et al., 2011, p. 4). It is given either in amperes or as a percentage of the coil current to the resonance point. Detuning value as amperes can be calculated as follows:

$$\begin{aligned} I_v &= I_{CoilTot} - I_{cNet} = I_{Coil} - I_{EFNet} = I_{Coil} - I_{cNet} + I_{CoilNet} \\ &= (B_{Coil} - B_{cNet} + B_{CoilNet})U_{PE} \\ &= \left(\frac{1}{\omega_s L_{Coil}} + \frac{1}{\omega_s L_{CoilNet}} - \omega_s C_{Net}\right) U_{PE}, \end{aligned} \tag{1}$$

where I_v is the system detuning, $I_{CoilTot}$ is the inductive current produced by all the connected ASCs, including distributed coils, I_{cNet} is the capacitive earth fault current produced by the network, I_{Coil} is the inductive current produced by the central ASC, I_{EFNet} is the capacitive earth fault current seen by central ASC, $I_{CoilNet}$ is the inductive current produce by the distributed compensation, B_{Coil} is the inductive susceptance of the central ASC, B_{cNet} is the capacitive susceptance of the network, $B_{CoilNet}$ is the inductive susceptance of the distributed coils, U_{PE} is the rated phase-to-ground voltage of the network, ω_s is the synchronous angular frequency of the system, L_{Coil} is the inductance of the central ASC, $L_{CoilNet}$ is the inductance of the distributed compensation, and C_{Net} is the phase-to-ground capacitance of the network.

A positive detuning value indicates that the network is over-compensated, and a negative value refers to under-compensation. The target detuning value is typically chosen so that the network is operated slightly over-compensated, typically 5 to 15 A in European utilities (Wahlroos et al., 2021, p. 4). This is because the resonance is generally undesirable as it causes overvoltages and amplifies harmonics in the network (Wahlroos et al.,

2011, p. 4–5). However, if the detuning deviates from the resonance by more than 25%, it can lead to high fault currents (Lakervi & Holmes, 1995, p. 43).

2.4 Tuning of arc suppression coil

When changes in the network occur, the size of the galvanically connected network changes. As the distribution lines have a specific line-to-earth capacitance per kilometer, the total line-to-earth capacitance of the network varies depending on the network topology. Therefore, the tuning of the ASC must correspond to the current network topology, which means that typically after a change in the network topology, the ASC must be retuned. To address this, numerous tuning methods have been developed to automatically determine the position of the ASC, i.e., the required inductive current.

Often the centralized compensation coil is equipped with an automatic tuning device, also known as the automatic regulator, to ensure that ASC is properly tuned at all times, regardless of changes in the network topology (Mäkinen, p.180). Therefore, when changes in the network topology occur, the automatic tuning device adjusts the inductance of the compensation coil so that the desired level of detuning is maintained. However, it should be noted that the set detuning value is valid only after a successful tuning procedure. Furthermore, the compensation coil must be adjustable for tuning, and often the tuning is based on motor-controlled adjustment of the coil air gap.

2.5 Network zero-sequence losses

The zero-sequence losses of the network, also known as shunt losses, are commonly referred to as system damping because they dampen the oscillations and transients during faults and after their disconnection (Wahlroos et al., 2021, p. 3). Network damping value I_d expressed in terms of currents in percent or amperes, is the sum of the total

shunt losses of the network. This includes the shunt losses of the feeders, losses of the ASC, and the parallel resistor (Wahlroos et al., 2021, p. 3). Damping is generally related to the size of the network's phase-to-ground capacitances and coil currents, and thus, damping increases in larger networks (Wahlroos et al., 2021, p. 8).

In practical networks, the phase-to-ground admittances are not ideal capacitances but rather include also resistive shunt losses, which are always present. The resistive shunt losses of conductors and insulators are typically only a few percent, 1–10 % of the capacitive component (Wahlroos et al., 2021, p. 2). Especially in modern cables, the resistive leakage current is very small due to the high quality of the insulating materials.

In addition, all the connected ASCs, both centralized and distributed, introduce shunt losses. The shunt losses of ASC are a function of coil current, typically 1–5 % of the inductive current (Wahlroos et al., 2021, p. 7). Furthermore, the resistive shunt losses can be intentionally increased by connecting the parallel resistor, which typically contributes 5–15 A of additional resistive current at the primary voltage level (Wahlroos et al., 2021, p. 4).

3 The natural healthy state zero-sequence voltage

The natural healthy state zero-sequence voltage, also known as neutral point voltage, neutral-to-earth voltage, neutral voltage displacement (NVD), neutral point displacement voltage (NPDV), and residual voltage, is a significant parameter that describes the compensated network. The natural healthy state zero-sequence voltage is introduced by the natural phase admittance unbalance, also referred to as asymmetry of the system, as in practical networks, the phase-wise network line-to-earth admittances are not precisely equal (Wahlroos et al., 2021, p. 8). In addition, traditional coil tuning algorithms also require sufficient natural zero-sequence voltage in the network.

The unbalance of line-to-earth admittances in the system varies with the active system topology. Typically, the natural healthy state zero-sequence voltage is 1–15 % of the system's nominal phase voltage at resonance (Wahlroos, 2023, p. 41). In a 20 kV medium voltage system, this means that zero-sequence voltage is typically 0,1–2 kV at resonance.

3.1 Fundamentals of the neutral point voltage

The fundamentals of the neutral point voltage and parameters influencing the neutral point voltage in compensated networks can be studied with a simple three-phase equivalent circuit of a distribution network, as illustrated in Figure 3 (Druml et al., 2001, pp. 1–2; Druml & Seifert, 2005, p. 2). The equivalent circuit of the network consists of a single feeder that represents all the feeders in the substation, which are galvanically connected. The feeder is presented with phase-to-ground admittances neglecting line series impedances as their values are very small compared with the shunt admittances. Also, the loads and phase-to-phase capacitances are disregarded as they do not contribute to the zero-sequence currents. The system's neutral point N is earthed via the compensation coil, including the parallel resistor.

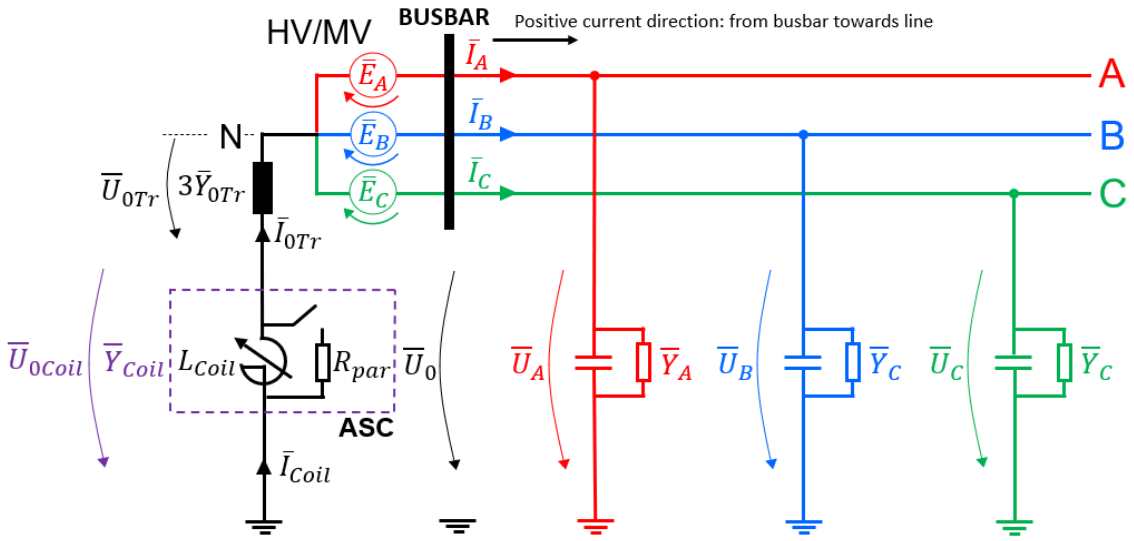

Figure 3. Three-phase equivalent circuit of the compensated distribution network.

In Figure 3, the following parameters at the primary voltage level are used:

- $\overline{E}_A$, $\overline{E}_B$, and $\overline{E}_C$ are the operating voltages of phases A, B, and C, respectively
- $\overline{I}_{0Tr}$ is the zero-sequence current of the earthing or main transformer
- $\overline{I}_A$, $\overline{I}_B$, and $\overline{I}_C$ are the line currents of phases A, B, and C, respectively
- $\overline{I}_{Coil}$ is the zero-sequence current measured at coil
- $\overline{U}_0$ is the zero-sequence voltage measured at busbar
- $\overline{U}_{0Coil}$ is the zero-sequence voltage measured at coil
- $\overline{U}_{0Tr}$, is the zero-sequence voltage across the earthing or main transformer
- $\overline{U}_A$, $\overline{U}_B$, and $\overline{U}_C$ are the phase-to-ground voltages of phases A, B, and C, respectively
- $\overline{Y}_{0Tr}$ is the zero-sequence admittance of earthing transformer per phase
- $\overline{Y}_A$, $\overline{Y}_B$, and $\overline{Y}_C$ are the phase-to-ground admittances of phases A, B, and C, respectively
- $\overline{Y}_{Coil}$ is the admittance of the ASC, including the conductance of parallel resistor

The phase-to-ground voltages of the compensated network are formed by the operating phase voltages at the secondary side of the main transformer, which are further affected by the neutral point voltage and can be expressed as follows:

$$\overline{U}_A = \bar{E}_A + \bar{U}_0, \tag{2}$$

$$\overline{U}_B = \bar{E}_B + \bar{U}_0, \tag{3}$$

$$\overline{U}_C = \bar{E}_C + \bar{U}_0. \tag{4}$$

Based on the previous expressions, the neutral point voltage of the network may be expressed mathematically as follows:

$$\overline{U}_0 = \frac{\overline{U}_A + \overline{U}_B + \overline{U}_C}{3}. \tag{5}$$

The total phase-to-ground admittance of the network $\overline{Y}_{Net}$ is the sum of phase-to-ground admittances:

$$\overline{Y}_{Net} = \overline{Y}_A + \overline{Y}_B + \overline{Y}_C, \tag{6}$$

where the phase-to-ground admittances can be expressed as complex phasors as follows for phase A:

$$\overline{Y}_A = G_A + jB_A = \frac{1}{R_A} + j\omega_s C_A, \tag{7}$$

where G_A is the phase-to-ground conductance of the phase A, B_A is the phase-to-ground susceptance of the phase A, and R_A is the phase-to-ground resistance of phase A.

A further simplification can be made by assuming that the unbalance of the line-to-earth admittances of the system is concentrated in phase A (Druml et al., 2001, p. 2; Druml & Seifert, 2005, p. 2). This definition can be used to describe the asymmetry of any arbitrary network. The equivalent circuit based on this definition is illustrated in Figure 4, where the phase-to-ground admittances of the system are described by the following expressions:

$$\overline{Y}_A = \overline{Y}_{asymm} + \frac{\overline{Y}_{symm}}{3}, \tag{8}$$

$$\overline{Y}_B = \frac{\overline{Y}_{symm}}{3}, \tag{9}$$

$$\overline{Y}_C = \frac{\overline{Y}_{symm}}{3}, \tag{10}$$

where $\overline{Y}_{asymm}$ is the asymmetrical phase-to-ground admittance and $\overline{Y}_{symm}$ is the symmetrical phase-to-ground admittance. Based on the previous expressions, the asymmetrical admittance may be expressed mathematically as follows:

$$\overline{Y}_{asymm} = \bar{Y}_A + \bar{a}^2 \cdot \bar{Y}_B + \bar{a} \cdot \bar{Y}_C. \tag{11}$$

where the phase shift operator is defined as:

$$\bar{a} = \cos(120^{\circ}) + j \cdot \sin(120^{\circ}). \tag{12}$$

The total phase-to-ground admittance of the network $\overline{Y}_{Net}$ is then the sum of the asymmetrical and symmetrical parts, as follows:

$$\overline{Y}_{Net} = \overline{Y}_{asymm} + \overline{Y}_{symm}. \tag{13}$$

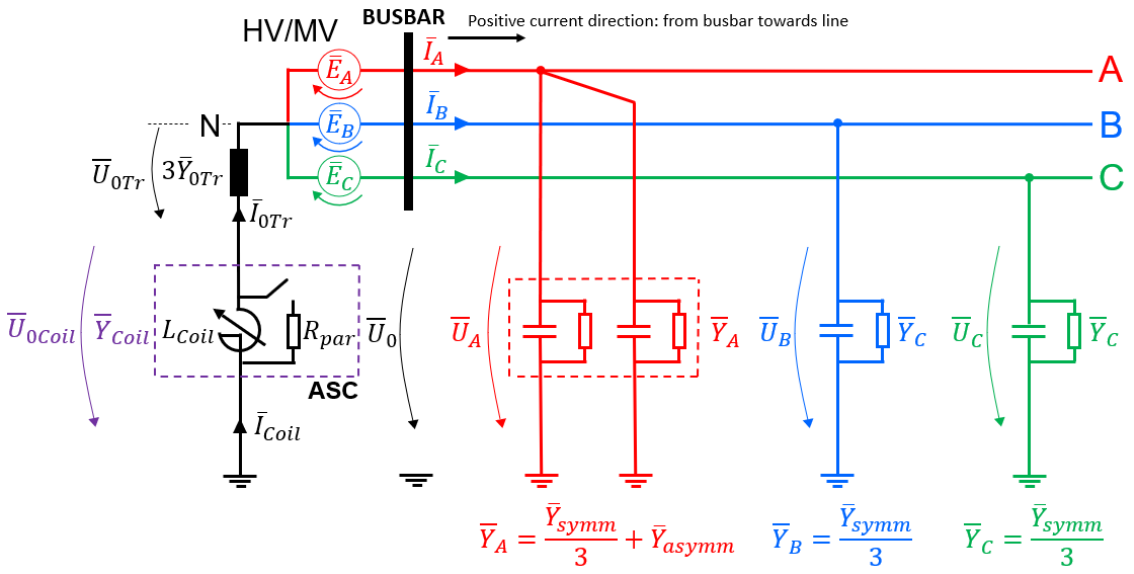

Figure 4. Three-phase equivalent circuit of the compensated distribution network when asymmetry is concentrated into phase A.

Figure 5 shows the single-phase equivalent circuit reduced from the three-phase equivalent in Figure 4. By neglecting the zero-sequence admittance $\overline{Y}_{0Tr}$ of the earthing or main transformer as its effect is minimal (see Section 2.1.1), the system in Figure 5 can be described by the following equation:

$$-\overline{U}_0\overline{Y}_{Coil} = (\overline{U}_0 + U_{PE})\overline{Y}_{asymm} + \overline{U}_0\overline{Y}_{symm}. \tag{14}$$

The fundamental equation describing the behavior of neutral point voltage can then be solved from (14) as follows:

$$\begin{aligned}\overline{U}_0 &= -U_{PE}\frac{\overline{Y}_{asymm}}{\overline{Y}_{asymm} + \overline{Y}_{symm} + \overline{Y}_{Coil}} = -U_{PE}\frac{\overline{Y}_{asymm}}{\overline{Y}_{Net} + \overline{Y}_{Coil}} \\ &= -U_{PE}\frac{\overline{Y}_{asymm}}{G_{Net} + G_{Coil} + j\left(\omega_s C_{Net} - \frac{1}{\omega_s L_{Coil}}\right)},\end{aligned} \tag{15}$$

where, G_{Net} is the phase-to-ground conductance, i.e., shunt losses, of the network and G_{Coil} is the conductance of the parallel resistor.

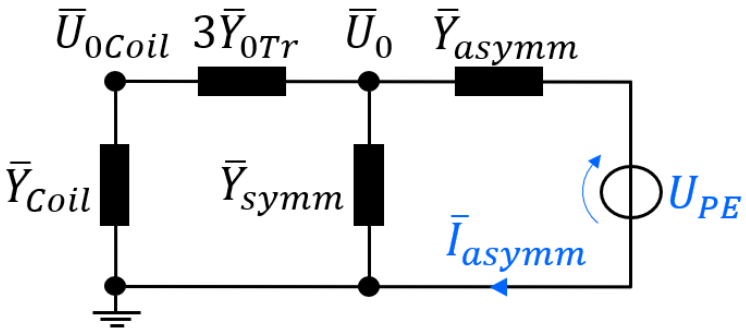

Figure 5. Single-phase equivalent circuit of the compensated distribution network when asymmetry is concentrated into phase A.

As introduced by Wahlroos et al. (2021, p. 8), the admittances of equations (15) can be expressed in terms of currents multiplying them with rated phase-to-ground voltage U_{PE} resulting the final form:

$$\overline{U}_0 = -U_{PE}\frac{\bar{I}_{asymm}}{I_d - j \cdot I_v}, \tag{16}$$

where I_d is the total shunt losses of the system, i.e., system damping and $\bar{I}_{asymm}$ represents the asymmetrical phase-to-ground admittance in terms of amperes. Alternatively, the equation (15) can also be expressed in terms of individual phase-to-ground admittances by using the definition (11), as follows:

$$\overline{U}_0 = -U_{PE}\frac{\bar{Y}_A + \bar{a}^2 \cdot \bar{Y}_B + \bar{a} \cdot \bar{Y}_C}{\overline{Y}_A + \overline{Y}_B + \overline{Y}_C + \bar{Y}_{Coil}}. \tag{17}$$

Further, Wahlroos et al. (2021, p. 8) describe that based on the expression (16), the magnitude of the zero-sequence voltage depends on the following three parameters:

- $\bar{I}_{asymm}$, the asymmetrical current, which is introduced by the unbalance of the phase-to-ground admittances. The higher the unbalance, the higher the zero-sequence voltage $\overline{U}_0$.
- I_d, the magnitude of the system damping. The lower the damping, the higher the zero-sequence voltage $\overline{U}_0$.
- I_v, the magnitude of the system detuning. The closer the detuning is to zero, the higher the zero-sequence voltage $\overline{U}_0$.

3.2 Resonance curve

Figure 6 illustrates the magnitude of healthy state zero-sequence voltage as a function of the system detuning, commonly known as the resonance curve. Alternatively, the resonance curve is also commonly given as a function of ASC current. It is essential to note that while the resonance curve is determined in a healthy network state, it is also valid during the earth fault, with the only difference being a higher voltage level.

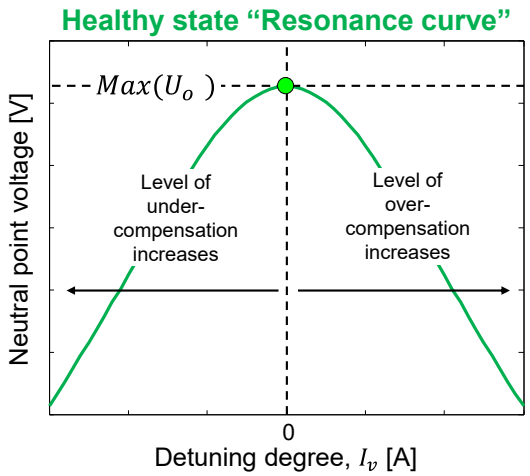

Figure 6. Resonance curve valid for the compensated network (Wahlroos et al., 2021, p. 9).

The system detuning determines the location of the resonance curve peak, while the system damping determines the height of the curve. The peak of the resonance curve,

i.e., the zero-sequence voltage at resonance, can be obtained from expression (16) as follows:

$$\max(U_0)\,[pu] = \left|\frac{\bar{I}_{asymm}}{I_d}\right|. \tag{18}$$

Furthermore, when the zero-sequence admittance of the earthing transformer is accounted for, the expression (15) has the following form:

$$\overline{U}_0 = -\frac{U_{PE}\bar{Y}_{asymm}(3\bar{Y}_{0Tr} + \bar{Y}_{Coil})}{(\bar{Y}_{asymm} + \bar{Y}_{symm} + 3\bar{Y}_{0Tr})\bar{Y}_{Coil} + 3\bar{Y}_{0Tr}(\bar{Y}_{asymm} + \bar{Y}_{symm})}. \tag{19}$$

Based on equation (19), it is not obvious how the resonance curve is affected by the inductive current produced by the admittance of the earthing transformer. However, it can be concluded that decreasing the admittance (increasing the impedance) of the earthing transformer shifts the location of the resonance point so that obtaining the resonance requires more inductive current produced by the ASC. More specifically, due to the admittance of the earthing transformer, the resonance curve shifts slightly to the right in Figure 6.

3.3 Traditional arc suppression coil tuning algorithms

The traditional ASC tuning algorithms utilize the movement of the ASC position and the natural zero-sequence voltage present in the network to determine the resonance point or to calculate the network's parameters. At its simplest, the regulator does not need to calculate the network parameters, as the position of the ASC can be adjusted step by step in the direction where the zero-sequence voltage of the network increases (ABB, 2004, pp. 1–2). This process continues until the zero-sequence voltage decreases, at

which point the maximum point of the zero voltage is passed, and the ASC position is adjusted one step back.

The position of the ASC, i.e., the required inductive current, can also be determined by calculating the values of the network parameters by minor coil movements (Trench Group, p. 4). The coil position is changed so that measured pairs of coil position and zero-sequence voltage ($\overline{I}_{Coil}$, $\overline{U}_0$) are evaluated by the chosen mathematical model of the resonance circuit, thus resulting desired network solution, e.g., system damping, detuning, and asymmetry (Schlömmer et al., 2017, pp. 1–2; Trench Group, p. 4). E.g., ABB's (2023, pp. 1730, 1736–1738) ASC tuning function PASANCR of the REX640 protection relay calculates the network parameters based on forced changes in the zero-sequence voltage obtained by adjusting the position of the ASC or changing the connection state of the parallel resistor.

However, using the previous methods makes it difficult to react quickly to changes in the network because the tuning principles are slow, as they involve additional coil movements. In addition, the tuning requires a sufficient level of natural zero-sequence voltage. According to the technical manual of the REX640 protection relay, the PASANCR function requires that the natural zero-sequence voltage reaches at least 0,5 % of the nominal phase-to-ground voltage at the network's resonance point (ABB, 2023, p. 1757). Furthermore, Druml et al. (2005, p.2) highlight that, especially in symmetrical networks, the resulting relative changes of the zero-sequence voltage due to the crosstalk become very large and are not negligible. As a result, the network's parameter estimation is more difficult due to disturbances.

4 Auxiliary zero-sequence current signal injection theory

This chapter introduces the concept, theory, and implementation of auxiliary zero-sequence current signal injection via power auxiliary winding (PAW) of the ASC in compensated distribution networks, referred to as current injection in this thesis. Therefore, the current injection theory is described and derived specifically when current is injected into the zero-sequence system through the network's neutral point. Additionally, the major applications of current injection are briefly introduced.

The injection theory describes the impact of current injection on a compensated distribution network by deriving relevant equations and equivalent circuits that describe the system's response to the injection. The parameters that affect the outcome of the injection are also highlighted and discussed. Moreover, the injection of fundamental frequency (mains frequency, synchronous frequency) and non-fundamental frequencies (frequencies unequal to the system's fundamental frequency) are considered separately so that the derived equivalent circuits and frequency domain equations do not mix different frequencies.

4.1 Basics of current injection

The idea of current injection is to supply alternating current into the zero-sequence system of the network, thus enabling desired functionalities or calculations of a given application. At most straightforward, this is implemented by injecting alternating current into the power auxiliary winding (PAW) of an ASC of suitable rated power. Figure 7 shows a three-phase equivalent circuit of compensated distribution network with an operating injection device.

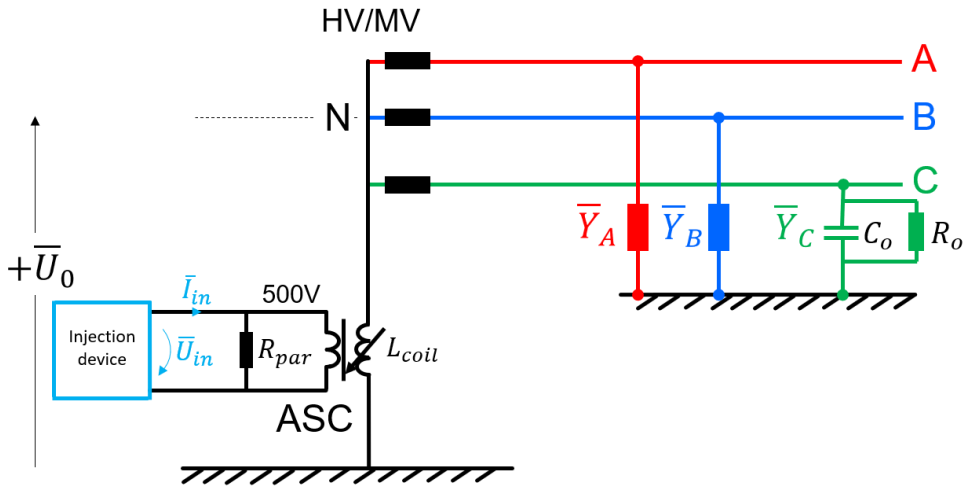

Figure 7. Simplified three-phase equivalent circuit of the compensated distribution network with an operating injection device.

The injected signal can be produced in several ways. At most straightforward, the power auxiliary transformer at the substation can operate as a voltage source at the fundamental frequency. The simplest way to generate other frequencies is to use a standard frequency converter, e.g., an H-bridge converter, that is further modified to fit the application (Talla et al., 2016, p. 387; Druml et al., 2005, pp. 3–4). Alternatively, a much cheaper version to generate a current with several frequencies can be implemented by pulsing a fundamental frequency signal using a thyristor unit (A. Eberle Gmbh & Co.KG, 2017, pp. 189–190; Trench Group, p. 3). These multi-frequency-based current injection solutions are described further in Sections 6.2 and 6.3.

4.2 Applications of current injection

The current injection is an essential method addressing various complex applications in compensated networks. These include the following applications:

- Tuning of arc suppression coil
- High impedance fault (HIF) detection
- Earth fault locating

- Residual current compensation (RCC)

Chapter 6 provides a detailed review of the arc suppression coil tuning, while the other applications are briefly introduced in the following subsections.

4.2.1 High impedance earth fault detection

Detecting high impedance earth fault, also known as high ohmic earth fault detection and high impedance fault (HIF) detection, is difficult due to the low fault current and zero-sequence voltage during the earth fault (Hänninen, 2001, p. 41). In a HIF, the zero-sequence impedance, i.e., the phase-to-ground impedance, of the faulty feeder is determined by the parallel connection of the fault resistance and the phase-to-ground impedance of the faulty feeder. This leads to a notable reduction in the zero-sequence impedance of the faulty feeder, while the zero-sequence impedances of the healthy feeders remain unaffected (Yu et al., 2022, p. 2). Further, the zero-sequence impedance of the entire network is reduced.

A known method for detecting high-impedance faults was introduced in an early patent by Druml and Papp (1996). The method utilizes a change in the zero-sequence voltage and zero-sequence currents of the feeders to calculate relevant components of the earth fault circuit, including the fault resistance. The change in the zero-sequence voltage can be achieved by adjusting the position of the ASC or injecting an auxiliary current at fundamental frequency into the neutral point or one of the phases. Additionally, the method enables the identification of the faulty phase.

The network parameter estimation for the ASC tuning based on injecting two frequencies, which will be introduced with further details in Section 6.2.1, can be extended to individual feeders by measuring the injected currents in each feeder, thus allowing the detection of the faulty feeder (Druml & Seifert, 2005, p. 5). More information on the

method can be found in the patent by Druml and Kugi (2007). Furthermore, without individual feeder measurements, the total phase-to-ground impedance of the network can be estimated, thus allowing for HIF detection at the system level. This is demonstrated in (Yu et al., 2022), where the damping rate of the network's estimated total zero-sequence admittance is evaluated before and after the fault.

4.2.2 Earth fault locating

Identifying and locating earth faults accurately is essential for maintaining safety and ensuring the overall stability and power quality of the network. Various techniques have been developed to locate earth faults accurately, including injection-based methods (Farughian et al., 2018; Buigues et al., 2012; Habib, 2022, pp. 17–18, Levashov et al., 2021). A common existing approach involves injecting a signal at the primary substation, typically via an arc suppression coil, and tracking the signal along the faulty feeder (Sheta et al., 2020, p. 17; Raunig et al., 2010). Druml et al. (2012; 2013) and Tengg et al. (2013) extend the concept of the fast pulsed zero-sequence current injection method used for the ASC tuning, which will be introduced with further details in Section 6.2, to earth fault localization based on zero-sequence current RMS (Root Mean Square) measurements. However, the injection is done during an earth fault with a much higher current compared to applications such as coil tuning and HIF detection, typically 1 to 5 A on the primary side (Druml et al., 2012, p. 3).

4.2.3 Residual current compensation

The concept of residual current compensation (RCC), i.e., earth fault neutralizing, is based on the fact that a traditional ASC can not compensate for the resistive and harmonic earth fault currents (Wang et a., 2016, p. 929). However, by injecting a controlled high-power current into the zero-sequence system of the network, the voltage of the faulted phase is forced to zero so that the earth fault current is also limited to zero

(Levashov et al., 2021, p. 3). This technique allows for reducing or eliminating the zero-sequence voltage, effectively neutralizing the earth fault. More information can be found in (Yang et al., 2019; Wang et al., 2016; Janssen et al., 2003; Levashov et al., 2021; Schiner & Schlömmer, 2022).

4.3 Electric circuit modeling of the injection device

This thesis considers two ways to model the injection device in an electrical circuit using the basic components:

- A current source
- A voltage source in series with a source impedance

These are further illustrated in Figure 8. The correct modeling depends on the actual implementation of the injection device, e.g., the modeling of the semiconductor-based injection device, such as a frequency converter, depends on the control of the device.

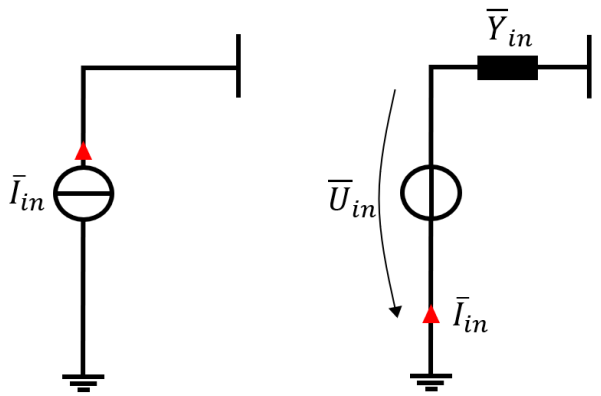

(a) Current source

(b) Voltage source in series with source impedance

Figure 8. Simplified electrical models of the injection device.

One significant difference between these models is how the injection device is interpreted from the system perspective. The current source is seen as an open circuit from

a system perspective, and correspondingly, the voltage source is seen as a short circuit that is limited by the source impedance. This difference is significant because, during the injection, the natural zero-sequence voltage of the system is connected between the terminals of the injection device in the PAW of the ASC, e.g., at 500 V level. This will result a leakage current through the injection device in case of injection device being presented as a voltage source.

4.4 Fundamental frequency injection

Fundamental frequency injection refers to an operation where alternating current is injected into the compensated network's zero-sequence system at the system's fundamental frequency. Thus, the frequency of the injected current is 50 or 60 Hz, depending on the operating fundamental frequency of the system. In this case, producing the injected signal is simpler because there is no need to generate sufficiently high non-fundamental frequency signals.

4.4.1 Equivalent circuits valid for fundamental frequency injection

The operation of fundamental frequency injection and its impact on the system can be studied with a simple three-phase equivalent circuit of a distribution network with an operating injection device presented as a current or voltage source, as illustrated in Figures 9 and 10, respectively. As discussed in Chapter 3, the equivalent scheme neglects loads, line series impedances, and phase-to-phase capacitances. Further, the natural asymmetry present in real networks due to differences in individual phase admittances is presented with asymmetric admittance concentrated into phase A. This simplification was further discussed in Section 3.1.

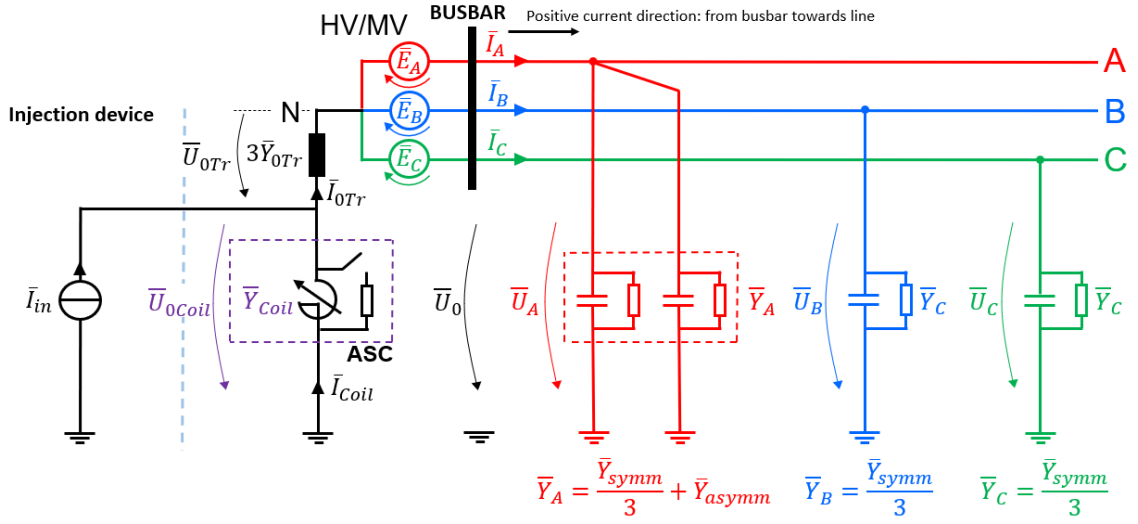

Figure 9. A three-phase equivalent circuit of the compensated distribution network with an operating injection device presented as a current source when asymmetry is concentrated into phase A.

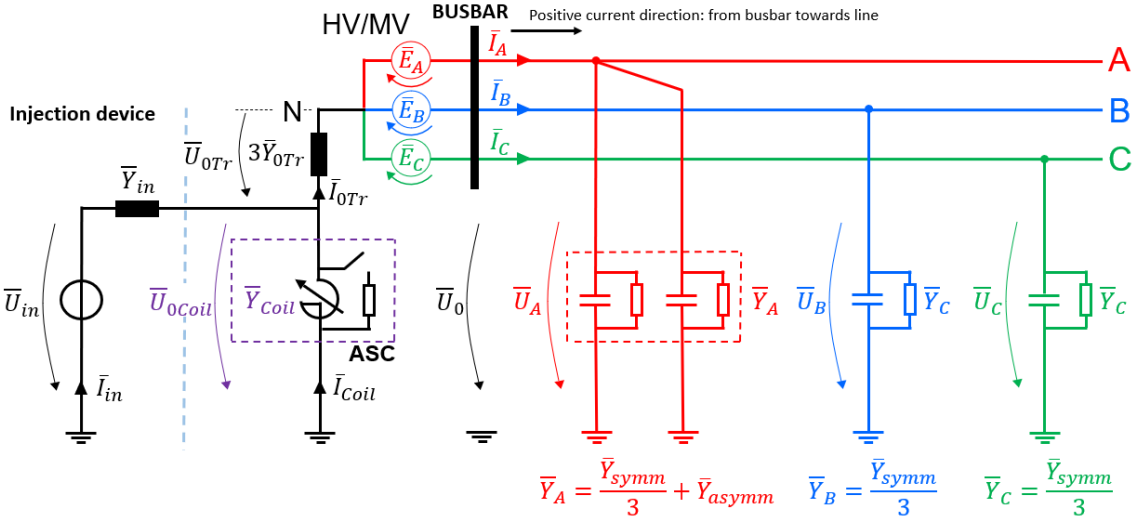

Figure 10. A three-phase equivalent circuit of the compensated distribution network with an operating injection device presented as a voltage source with a series source impedance when asymmetry is concentrated into phase A.

In Figures 9 and 10, the following parameters at the primary voltage level are used:

- $\bar{I}_{in}$ is the current produced by the injection device or the total current that flows through the injection device, depending on the presentation of the injection device

- $\overline{U}_{in}$ is the source voltage of voltage source-based injection
- $\overline{Y}_{in}$ is the source admittance of the injection device

The following equation can be written to describe the system:

$$\overline{I}_{0Tr} = \overline{I}_A + \overline{I}_B + \overline{I}_C. \tag{20}$$

Equation (20) can further be developed as shown in the following expressions:

$$\overline{I}_{0Tr} = \overline{Y}_A\overline{U}_A + \overline{Y}_B\overline{U}_A + \overline{Y}_C\overline{U}_C, \tag{21}$$

$$\overline{I}_{0Tr} = \left(\frac{\overline{Y}_{symm}}{3} + \overline{Y}_{asymm}\right)\overline{U}_A + \left(\frac{\overline{Y}_{symm}}{3}\right)\overline{U}_A + \left(\frac{\overline{Y}_{symm}}{3}\right)\overline{U}_C, \tag{22}$$

$$\overline{I}_{0Tr} = \left(\frac{\overline{Y}_{symm}}{3} + \overline{Y}_{asymm}\right)\left(\overline{E}_A + \overline{U}_0\right) + \left(\frac{\overline{Y}_{symm}}{3}\right)\left(\overline{E}_B + \overline{U}_0\right) + \left(\frac{\overline{Y}_{symm}}{3}\right)\left(\overline{E}_C + \overline{U}_0\right), \tag{23}$$

$$\overline{I}_{0Tr} = \left(\frac{\overline{Y}_{symm}}{3} + \overline{Y}_{asymm}\right)\left(U_{PE} + \overline{U}_0\right) + \left(\frac{\overline{Y}_{symm}}{3}\right)\left(\bar{a}^2 \cdot U_{PE} + \overline{U}_0\right) + \left(\frac{\overline{Y}_{symm}}{3}\right)\left(\bar{a} \cdot U_{PE} + \overline{U}_0\right). \tag{24}$$

Equation (24) uses the following definitions:

$$\overline{E}_A = U_{PE}, \tag{25}$$

$$\overline{E}_B = \bar{a}^2 \cdot U_{PE}, \tag{26}$$

$$\overline{E}_C = \bar{a} \cdot U_{PE}. \tag{27}$$

By simplifying, equation (24) reduces to the following form:

$$\overline{I}_{0Tr} = \overline{Y}_{asymm}\left(U_{PE} + \overline{U}_0\right) + \overline{Y}_{symm}\overline{U}_0. \tag{28}$$

Finally, by further developing equation (28) and using the definition (25), we obtain the following form that can be used to derive the single-phase equivalent circuits shown in Figures 11 and 12 for injections based on current and voltage sources, respectively:

$$\overline{I}_{in} - \overline{Y}_{Coil}\overline{U}_{0Coil} = \overline{Y}_{asymm}\left(\overline{E}_A + \overline{U}_0\right) + \overline{Y}_{symm}\overline{U}_0. \tag{29}$$

A similar configuration, as shown in Figure 11, is given in (Druml & Seifert, 2005, p. 4), which, however, neglects the resistive phase-to-ground losses of the feeders. In addition, it also indicates the connection of distributed compensation in parallel to shunt capacitances. In Figure 11, the inductive component of distributed compensation can be included in the symmetrical phase-to-ground admittance of the network $\overline{Y}_{symm}$.

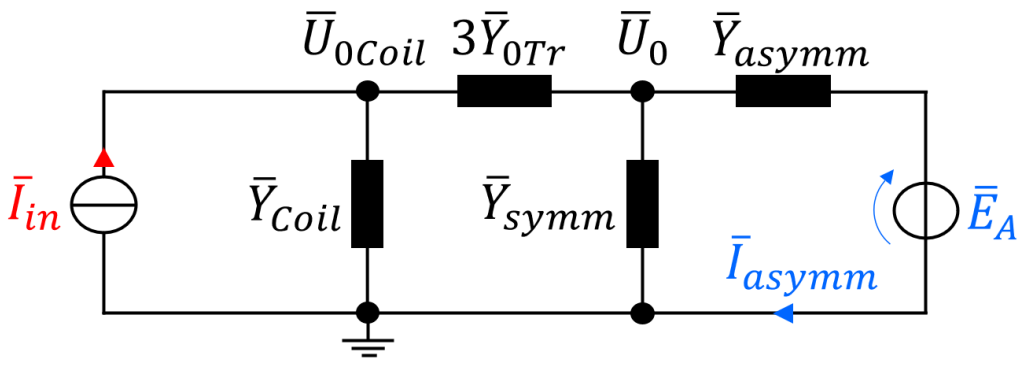

Figure 11. A single-phase equivalent circuit of compensated distribution network with an operating injection device presented as a current source. Valid for fundamental frequency injection.

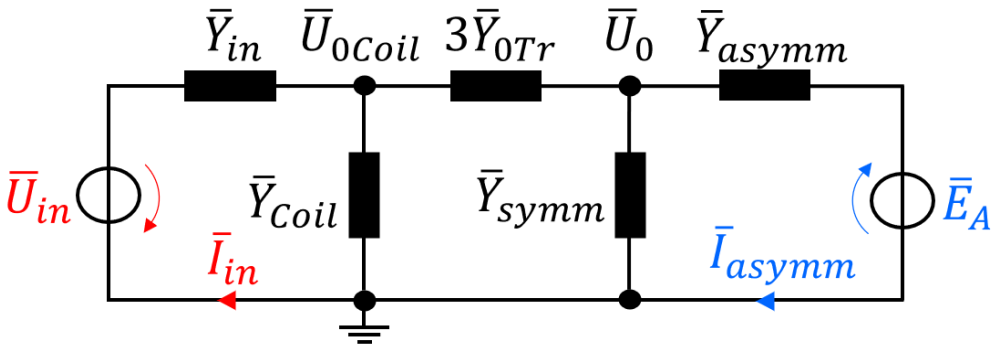

Figure 12. A single-phase equivalent circuit of compensated distribution network with an operating injection device presented as a voltage source with a series source admittance. Valid for fundamental frequency injection.

The single-phase equivalent circuit can be further simplified if the zero-sequence impedance of the earthing transformer is neglected, as shown in Figures 13 and 14. A similar simplified configuration, as illustrated in Figure 13, is widely shown in the literature by leading manufacturers and professionals (A. Eberle Gmbh & Co.KG, 2017, p. 183; Druml et al., 2005, p. 3; Trench Group, p. 4).

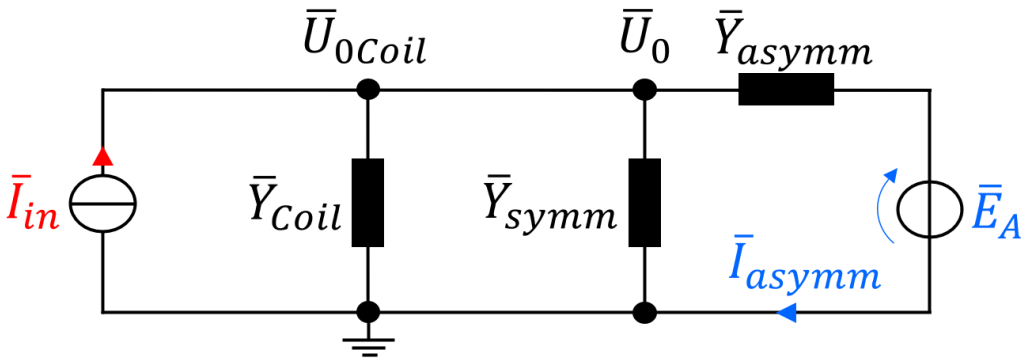

Figure 13. A single-phase equivalent circuit of compensated distribution network with a negligible zero-sequence impedance of the earthing transformer and an operating injection device presented as a current source. Valid for fundamental frequency injection.

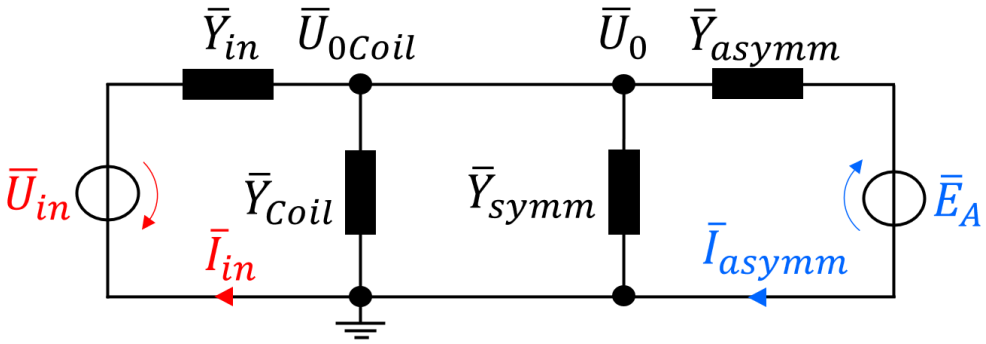

Figure 14. A single-phase equivalent circuit of compensated distribution network with a negligible zero-sequence impedance of the earthing transformer and an operating injection device presented as a voltage source with a series source impedance. Valid for fundamental frequency injection.

Based on Figures 12 and 14, when the injection device is presented as a voltage source and serial admittance, the current that flows through the injection device consists of both the current produced by the source voltage of the injection and the current due to the natural zero-sequence voltage of the network. As a result, the zero-sequence voltage due to natural asymmetry is decreased by the leakage current through the injection device during the injection.

4.4.2 Equations valid for fundamental frequency injection

This section presents the equations that describe the system behavior during fundamental frequency injection. These equations can be derived based on the equivalent circuits valid for fundamental frequency injection when the system is described based on symmetric and asymmetric line-to-ground admittances. The derived equations are concentrated in Tables 1 and 2.

The equations presented in Table 1 can be applied to injections based on both current and voltage sources and thus are valid for Figures 9–14. In this case, the injection based on the voltage source can be considered to operate so that desired current is obtained, i.e., in current control mode. Table 2 includes equations valid for voltage-controlled

injections, which only apply to voltage source-based injections shown in Figures 10, 12, and 14.

Table 1. Equations valid for current controlled fundamental frequency injection.

Zero-sequence voltage at busbar $\bar{U}_0$ as a function of injection current $\bar{I}_{in}$. I.e., the zero-sequence voltage at busbar due to injection current.

$$\bar{U}_0 = \frac{-\bar{Y}_{asymm}\bar{Y}_{Coil}\bar{E}_A - 3\bar{Y}_{0Tr}\bar{Y}_{asymm}\bar{E}_A + 3\bar{Y}_{0Tr}\bar{I}_{in}}{\bar{Y}_{asymm}\bar{Y}_{Coil} + 3\bar{Y}_{0Tr}\bar{Y}_{asymm} + 3\bar{Y}_{0Tr}\bar{Y}_{Coil} + \bar{Y}_{symm}\bar{Y}_{Coil} + 3\bar{Y}_{0Tr}\bar{Y}_{symm}} \tag{30}$$

Without the zero-sequence admittance $\bar{Y}_{0Tr}$.

$$\bar{U}_0 = \frac{-\bar{Y}_{asymm}\bar{E}_A + \bar{I}_{in}}{\bar{Y}_{asymm} + \bar{Y}_{symm} + \bar{Y}_{Coil}} = \frac{-\bar{Y}_{asymm}\bar{E}_A + \bar{I}_{in}}{G_{Net} + G_{Coil} + j\left(\omega_s C_{Net} - \frac{1}{\omega_s L_{Coil}}\right)}$$

$$= \frac{-\bar{Y}_{asymm}\bar{E}_A + \bar{I}_{in}}{I_d - j \cdot I_v} U_{PE} = \frac{-\bar{I}_{asymm}\bar{E}_A + \bar{I}_{in}U_{PE}}{I_d - j \cdot I_v} = \frac{-\bar{I}_{asymm} + \bar{I}_{in}}{I_d - j \cdot I_v} U_{PE} \tag{31}$$

Injection current $\bar{I}_{in}$ as a function of zero-sequence voltage $\bar{U}_0$. I.e., injection current needed to obtain a certain zero-sequence voltage.

$$\bar{I}_{in} = \frac{(3\bar{Y}_{0Tr} + \bar{Y}_{Coil})\left(\bar{Y}_{Net}\bar{U}_0 + \bar{Y}_{asymm}\bar{E}_A\right) + 3\bar{Y}_{0Tr}\bar{Y}_{Coil}\bar{U}_0}{3\bar{Y}_{0Tr}} \tag{32}$$

Without the zero-sequence admittance $\bar{Y}_{0Tr}$.

$$\bar{I}_{in} = \bar{Y}_{asymm}(\bar{U}_0 + \bar{E}_A) + \bar{Y}_{symm}\bar{U}_0 + \bar{Y}_{Coil}\bar{U}_0 \tag{33}$$

Zero-sequence voltage at coil $\bar{U}_{0Coil}$ as a function of injection current $\bar{I}_{in}$. I.e., the zero-sequence voltage at coil due to injection current.

$$\bar{U}_{0Coil} = \frac{3\bar{Y}_{0Tr}\left(\bar{I}_{in} - \bar{Y}_{asymm}\bar{E}_A\right) + \bar{I}_{in}\left(\bar{Y}_{asymm} + \bar{Y}_{symm}\right)}{3\bar{Y}_{0Tr}\left(\bar{Y}_{asymm} + \bar{Y}_{symm} + \bar{Y}_{Coil}\right) + \bar{Y}_{Coil}\left(\bar{Y}_{asymm} + \bar{Y}_{symm}\right)} \tag{34}$$

Without the zero-sequence admittance $\bar{Y}_{0Tr}$.

$$\bar{U}_{0Coil} = \bar{U}_0 = \frac{-\bar{Y}_{asymm}\bar{E}_A + \bar{I}_{in}}{\bar{Y}_{asymm} + \bar{Y}_{symm} + \bar{Y}_{Coil}} \tag{35}$$

Zero-sequence impedance seen from the terminals of the injection $\bar{Z}_{inj}$.

$$\bar{Z}_{inj} = \frac{\bar{U}_{0Coil}}{\bar{I}_{in}} = \frac{3\bar{Y}_{0Tr}\left(\bar{I}_{in} - \bar{Y}_{asymm}\bar{E}_A\right) + \bar{I}_{in}\left(\bar{Y}_{asymm} + \bar{Y}_{symm}\right)}{\left(3\bar{Y}_{0Tr}\left(\bar{Y}_{asymm} + \bar{Y}_{symm} + \bar{Y}_{Coil}\right) + \bar{Y}_{Coil}\left(\bar{Y}_{asymm} + \bar{Y}_{symm}\right)\right)\bar{I}_{in}} \tag{36}$$

Without the zero-sequence admittance $\bar{Y}_{0Tr}$.

$$\bar{Z}_{inj} = \frac{\bar{U}_{0Coil}}{\bar{I}_{in}} = \frac{-\bar{Y}_{asymm}\bar{E}_A + \bar{I}_{in}}{\left(\bar{Y}_{asymm} + \bar{Y}_{symm} + \bar{Y}_{Coil}\right)\bar{I}_{in}} = \frac{-\bar{Y}_{asymm}\bar{E}_A + \bar{I}_{in}}{(I_d - j \cdot I_v)\bar{I}_{in}} U_{PE} \tag{37}$$

Table 2. Equations valid for voltage-controlled fundamental frequency injection when the injection device is modeled as a voltage source.

Zero-sequence voltage at busbar $\bar{U}_0$ as a function of injection voltage $\bar{U}_{in}$. I.e., zero-sequence voltage at busbar due to injection source voltage.

$$\bar{U}_0 = \frac{3\bar{Y}_{0Tr}\bar{Y}_{in}\bar{U}_{in} - \bar{Y}_{asymm}\bar{E}_A(\bar{Y}_{in} + 3\bar{Y}_{0Tr} + \bar{Y}_{Coil})}{(\bar{Y}_{asymm} + \bar{Y}_{symm})(\bar{Y}_{in} + 3\bar{Y}_{0Tr} + \bar{Y}_{Coil}) + 3\bar{Y}_{0Tr}(\bar{Y}_{in} + \bar{Y}_{Coil})} \quad (38)$$

Without the zero-sequence admittance $\bar{Y}_{0Tr}$.

$$\bar{U}_0 = \frac{\bar{Y}_{in}\bar{U}_{in} - \bar{Y}_{asymm}\bar{E}_A}{\bar{Y}_{asymm} + \bar{Y}_{symm} + \bar{Y}_{Coil} + \bar{Y}_{in}} = \frac{\bar{Y}_{in}\bar{U}_{in} - \bar{Y}_{asymm}\bar{E}_A}{\bar{Y}_{in} + G_{Net} + G_{Coil} + j\left(\omega_s C_{Net} - \frac{1}{\omega_s L_{Coil}}\right)}$$

$$= \frac{\bar{Y}_{in}\bar{U}_{in} - \bar{Y}_{asymm}\bar{E}_A}{\bar{Y}_{in}U_{PE} + I_d - j\cdot I_v}U_{PE} = \frac{\bar{Y}_{in}\bar{U}_{in}U_{PE} - \bar{I}_{asymm}\bar{E}_A}{\bar{Y}_{in}U_{PE} + I_d - j\cdot I_v} = \frac{\bar{Y}_{in}\bar{U}_{in} - \bar{I}_{asymm}}{\bar{Y}_{in}U_{PE} + I_d - j\cdot I_v}U_{PE} \quad (39)$$

Injection current $\bar{I}_{in}$ as a function of injection source voltage $\bar{U}_{in}$. I.e., injection current due to injection source voltage.

$$\bar{I}_{in} = \frac{\bar{Y}_{in}\left(\left((\bar{U}_{in} + \bar{E}_A)\bar{Y}_{asymm} + \bar{U}_{in}(\bar{Y}_{Coil} + \bar{Y}_{symm})\right)3\bar{Y}_{0Tr} + \bar{U}_{in}\bar{Y}_{Coil}\bar{Y}_{Net}\right)}{3\bar{Y}_{0Tr}(\bar{Y}_{asymm} + \bar{Y}_{symm} + \bar{Y}_{Coil} + \bar{Y}_{in}) + (\bar{Y}_{asymm} + \bar{Y}_{symm})(\bar{Y}_{Coil} + \bar{Y}_{in})} \quad (40)$$

Without the zero-sequence admittance $\bar{Y}_{0Tr}$.

$$\bar{I}_{in} = \frac{\bar{Y}_{in}\left((\bar{Y}_{asymm} + \bar{Y}_{symm} + \bar{Y}_{Coil})\bar{U}_{in} + \bar{Y}_{asymm}\bar{E}_A\right)}{\bar{Y}_{asymm} + \bar{Y}_{symm} + \bar{Y}_{Coil} + \bar{Y}_{in}} \quad (41)$$

Injection source voltage $\bar{U}_{in}$ as a function of $\bar{U}_0$. I.e., injection source voltage needed to obtain a certain zero-sequence voltage.

$$\bar{U}_{in} = \frac{(3\bar{Y}_{0Tr} + \bar{Y}_{in} + \bar{Y}_{Coil})\left(\bar{Y}_{Net}\bar{U}_0 + \bar{Y}_{asymm}\bar{E}_A\right) + 3\bar{Y}_{0Tr}\bar{U}_0(\bar{Y}_{in} + \bar{Y}_{Coil})}{3\bar{Y}_{0Tr}\bar{Y}_{in}} \quad (42)$$

Without the zero-sequence admittance $\bar{Y}_{0Tr}$.

$$\bar{U}_{in} = \frac{\left(\bar{Y}_{asymm} + \bar{Y}_{symm} + \bar{Y}_{Coil} + \bar{Y}_{in}\right)\bar{U}_0 + \bar{Y}_{asymm}\bar{E}_A}{\bar{Y}_{in}} \quad (43)$$

Injection source voltage $\bar{U}_{in}$ as a function of injection current $\bar{I}_{in}$. I.e., injection source voltage needed to obtain a certain injection current.

$$\bar{U}_{in} = \frac{\left((\bar{Y}_{Net} + \bar{Y}_{Coil} + \bar{Y}_{in})\bar{I}_{in} - \bar{Y}_{in}\bar{Y}_{asymm}\bar{E}_A\right)3\bar{Y}_{0Tr} + \bar{I}_{in}\bar{Y}_{Net}(\bar{Y}_{Coil} + \bar{Y}_{in})}{3\bar{Y}_{0Tr}(\bar{Y}_{Net} + \bar{Y}_{Coil})\bar{Y}_{in} + \bar{Y}_{Coil}\bar{Y}_{Net}\bar{Y}_{in}} \quad (44)$$

Without the zero-sequence admittance $\bar{Y}_{0Tr}$.

$$\bar{U}_{in} = \frac{\left(\bar{Y}_{asymm} + \bar{Y}_{symm} + \bar{Y}_{Coil} + \bar{Y}_{in}\right)\bar{I}_{in} - \bar{Y}_{in}\bar{Y}_{asymm}\bar{E}_A}{\bar{Y}_{in}\left(\bar{Y}_{asymm} + \bar{Y}_{symm} + \bar{Y}_{Coil}\right)} \quad (45)$$

Based on the equation (31) in Table 1, when the zero-sequence admittance of earthing transformer is neglected, the system's response to the current-based fundamental frequency injection depends on the following parameters:

- The magnitude of the injected current $\bar{I}_{in}$.
- The phase shift of the injected current $\bar{I}_{in}$ in relation to the asymmetrical current $\bar{I}_{asymm}$. Therefore, the fundamental frequency injection can increase or decrease the natural zero-sequence voltage due to asymmetry, depending on the phase shift of the injection.
- $\bar{I}_{asymm}$, asymmetric current, introduced by the unbalance of the phase-to-ground admittances. The higher the unbalance, the higher the zero-sequence voltage $\overline{U}_0$ due to asymmetry.
- I_d, the magnitude of the system damping. The lower the damping, the higher the outcome of the injection.
- I_v, the magnitude of the system detuning. The closer the detuning is to zero, the higher the outcome of the injection.

Although the previous observations were made assuming that the zero-sequence admittance of the earthing transformer is negligible, they remain valid with a non-negligible admittance of the transformer. This is because, in practice, the zero-sequence admittance of the earthing transformer has only a minor impact on the results.

From the network's perspective, the power requirement of the injection increases based on the system damping I_d and detuning I_v. In practice, the system damping can not be influenced to reduce the power requirement of the injection, as it is an inherent trait of the network. However, the system detuning can be influenced by tuning the arc suppression coil so that the power requirement is minimal, i.e., the system is in resonance. This is further observed based on expression (37) in Table 1, as the magnitude of the zero-sequence impedance seen from the terminals of the injection $\bar{Z}_{inj}$ increases as the system detuning I_v decreases. Therefore, the load, i.e., impedance, of the injection is

highest when the system is in resonance, resulting the highest zero-sequence voltage response for current-based injection.

Similarly, when the injection device is presented as a voltage source and a serial admittance, based on the equation (39) in Table 2, the system's response to the voltage-based fundamental frequency injection depends on the system damping I_d, system detuning I_v, and asymmetry of phase-to-ground admittances $\bar{I}_{asymm}$. In addition, the outcome of the voltage-based injection depends on the following parameters:

- $\overline{U}_{in}$, the magnitude and phase shift of the source voltage of the injection. The injection can increase or decrease the natural zero-sequence voltage based on the phase shift.
- $\bar{Y}_{in}$, the source admittance of the injection. The higher the source admittance (lower source impedance), the higher the outcome of the injection. However, lower source admittance, i.e., higher source impedance, results less leakage current through the injection device due to natural zero-sequence voltage.

The source voltage of the injection can also be operated to produce a certain injection current, as illustrated by equations (44) and (45) in Table 2. In which case, the equations in Table 1 can be applied as the current flowing through the injection device is controlled to a specific value. Further, based on equation (16) and equation (39) in Table 2, during the injection, the zero-sequence voltage due to natural asymmetry is decreased as the source admittance of the injection is connected in parallel to the coil, decreasing the total zero-sequence impedance of the system.

Finally, it should be noted that if distributed compensation is present in the network, the capacitive current of the network appears smaller from the point of view of the injection, as the distributed compensation reduces it. Therefore, if distributed compensation is also considered, the total symmetric shunt admittance of the network $\bar{Y}_{Net}$ should be divided into inductive and capacitive parts, as follows:

$$\bar{Y}_{Net} = G_{Net} + jB_{cNet} - jB_{CoilNet} = G_{Net} + j\left(\omega_s C_{Net} - \frac{1}{\omega_s L_{CoilNet}}\right)$$
$$= G_{Net} + j\omega_s C_{EFNet} = G_{Net} + jB_{EFNet}, \quad (46)$$

where B_{EFNet} is the uncompensated capacitive susceptance of the network by the distributed compensation and C_{EFNet} is the uncompensated phase-to-ground capacitance of the network by the distributed compensation. Therefore, it should be noted, that equations (31), (37) in Tables 1 and 2 neglect the inductive part of the total shunt admittance of the network $B_{CoilNet}$ thus simplifying the expressions.

4.5 Injection of non-fundamental frequencies

Non-fundamental frequency injection refers to an operation where alternating current is injected into the zero-sequence system of the compensated network at one or more non-fundamental frequencies. Therefore, the injected current contains primarily frequencies other than the fundamental frequency of the system. Typically, for coil tuning application, the frequency of the injected signal is between 10–250 Hz. In addition, it should be noted that in this section, the admittances are scaled to the injection frequency in which point of view the system is analyzed.

4.5.1 Equivalent circuits valid for non-fundamental frequency injection

The operation of non-fundamental frequency injection can be studied based on the single-phase equivalent circuits of Section 4.3.1 valid for fundamental frequency injection by neglecting the phase A voltage source operating at the fundamental frequency. Hence, the system is analyzed at the frequency of the injected signal. As a result, the asymmetry of the network does not affect the outcome of the injection, and further simplification can be obtained by considering the expression (13). Finally, valid single-phase

equivalents are obtained for non-fundamental frequency injection, as shown in Figures 15 and 16 for current and voltage source based injections, respectively.

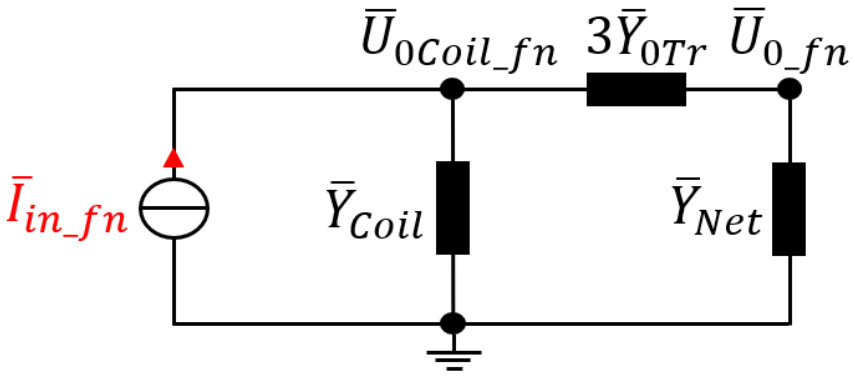

Figure 15. A single-phase equivalent circuit of compensated distribution network with an operating injection device presented as a current source. Valid for non-fundamental frequency injection.

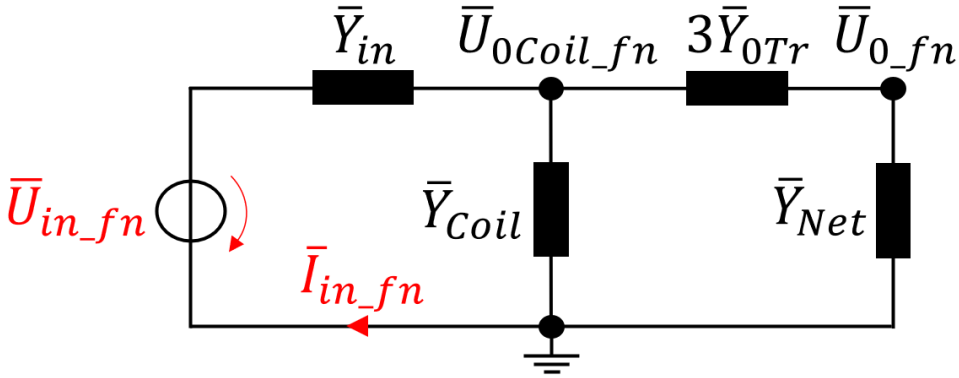

Figure 16. A single-phase equivalent circuit of compensated distribution network with an operating injection device presented as a voltage source with a serial source impedance. Valid for non-fundamental frequency injection.

In Figures 15 and 16, the following parameters at the primary voltage level are used:

- $\bar{I}_{in\_fn}$ is the current produced by the injection device at the frequency f_n
- $\bar{U}_{in\_fn}$ is the source voltage of voltage source-based injection operating at the frequency f_n
- $\bar{U}_{Coil\_fn}$ is the zero-sequence voltage measured at coil at the frequency f_n

- $\overline{U}_{0\_fn}$ is the zero-sequence voltage measured at busbar at the frequency f_n
- All the frequency-dependent admittances, i.e., $\overline{Y}_{in}$, $\overline{Y}_{Coil}$, $\overline{Y}_{0Tr}$, and $\overline{Y}_{Net}$, are scaled to the frequency of the injection f_n

When the zero-sequence admittance of the earthing transformer is disregarded, the single-phase equivalents are further reduced to the following forms illustrated in Figures 17 and 18. However, experience is shown that the effect of the transformer zero-sequence impedance is not negligible and can be significant at non-fundamental frequencies. Despite the previous, similar configurations, as shown in Figure 17, are widely used in the literature (A. Eberle Gmbh & Co.KG, 2017, p. 184; Druml et al., 2005, p. 3; Talla et al., 2016, p. 388).

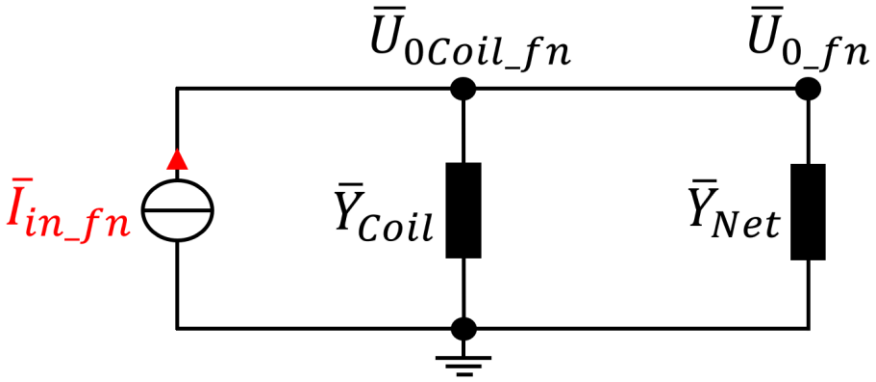

Figure 17. A single-phase equivalent circuit of compensated distribution network with a negligible zero-sequence impedance of the earthing transformer and an operating injection device presented as a current source. Valid for non-fundamental frequency injection.

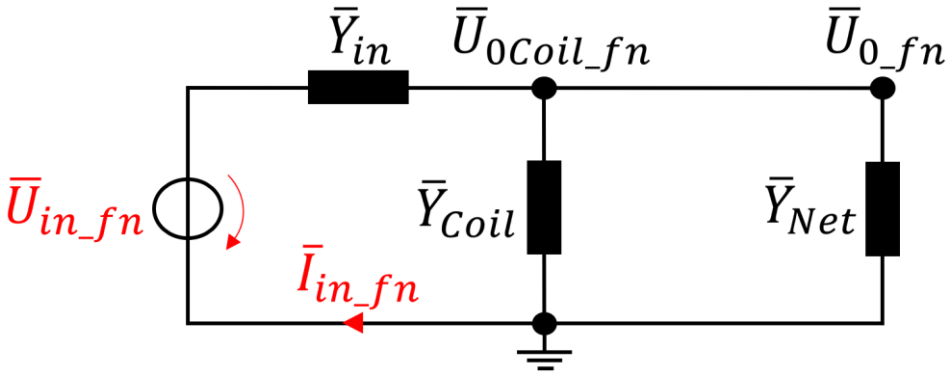

Figure 18. A single-phase equivalent circuit of compensated distribution network with a negligible zero-sequence impedance of the earthing transformer and an operating injection device presented as a voltage source and a series source impedance. Valid for non-fundamental frequency injection.

Additionally, the 50 Hz leakage current passing through the voltage source-based injection device due to natural asymmetry can be studied with the single-phase equivalents shown in Figures 19 and 20. In this case, the source admittance of the injection device presents the admittance in which the inverter-based injection device appears from the networks point of view at the fundamental frequency of the system.

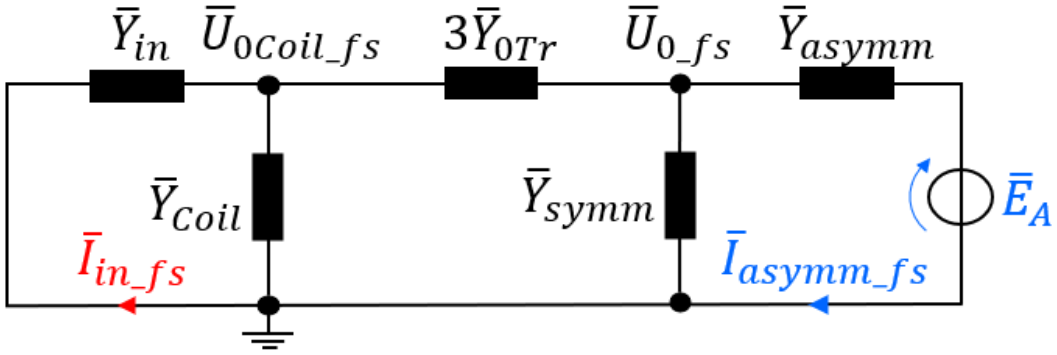

Figure 19. A single-phase equivalent circuit of compensated distribution network with an injection when the system is analyzed at the fundamental frequency. The injection device is presented as a voltage source with a series source impedance and operated at non-fundamental frequency.

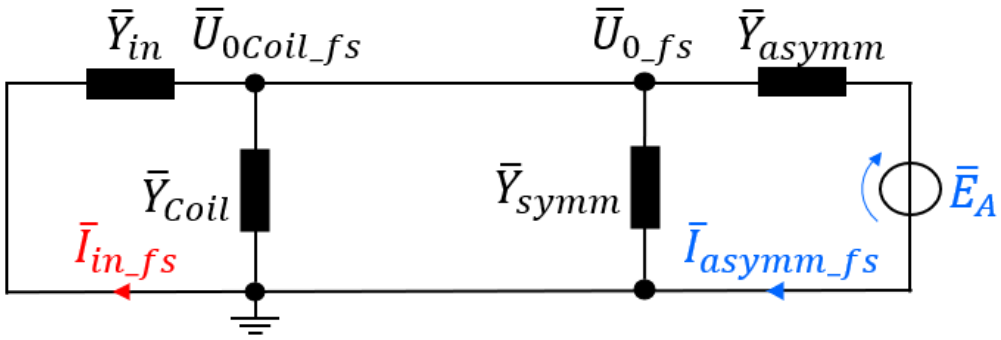

Figure 20. A single-phase equivalent circuit of compensated distribution network with injection and a negligible zero-sequence impedance of the earthing transformer when the system is analyzed at the fundamental frequency. The injection device is presented as a voltage source with series source impedance and operated at non-fundamental frequency.

In Figures 19 and 20, the following parameters at the primary voltage level are used:

- $\overline{I}_{in\_fs}$ is the current that flows through the injection device at the fundamental frequency of the system f_s during the injection
- $\overline{U}_{Coil\_fs}$ is the zero-sequence voltage measured at coil at the fundamental frequency of the system f_s during injection
- $\overline{U}_{0\_fs}$ is the zero-sequence voltage measured at busbar at the fundamental frequency of the system f_s during injection
- All the frequency-dependent admittances, i.e., $\overline{Y}_{in}$, $\overline{Y}_{Coil}$, $\overline{Y}_{0Tr}$, and $\overline{Y}_{Net}$, are scaled to the fundamental frequency of the system f_s

4.5.2 Equations valid for non-fundamental frequency injection

This section presents the equations that describe the system behavior during the non-fundamental frequency injection. These equations can be derived based on the equivalent circuits valid for non-fundamental frequency injection when the system is described based on symmetric and asymmetric line-to-ground admittances. The derived equations are concentrated in Tables 3, 4, and 5.

The equations presented in Table 3 can be applied to injections based on both current and voltage sources and thus are valid for Figures 15–18. In this case, the injection based on the voltage source operates in the current control mode. Table 4 includes equations valid for voltage-controlled injections that only apply to voltage source-based injections shown in Figures 16 and 18. Furthermore, the equations in Table 5 consider the influence of the leakage current at fundamental frequency during the voltage source-based non-fundamental frequency injection and therefore apply to Figures 19 and 20.

Table 3. Equations valid for current controlled non-fundamental frequency injection.

Zero-sequence voltage at busbar $\bar{U}_0$ as a function of injection current $\bar{I}_{in}$ at frequency f_n. I.e., the zero-sequence voltage at busbar due to injection current.

$$\bar{U}_{0\_fn} = \frac{3\bar{Y}_{0Tr}\bar{I}_{in\_fn}}{\bar{Y}_{Net}\bar{Y}_{Coil} + 3\bar{Y}_{0Tr}\bar{Y}_{Net} + 3\bar{Y}_{0Tr}\bar{Y}_{Coil}} \tag{47}$$

Without the zero-sequence admittance $\bar{Y}_{0Tr}$.

$$\bar{U}_{0\_fn} = \frac{\bar{I}_{in\_fn}}{\bar{Y}_{Net} + \bar{Y}_{Coil}} = \frac{\bar{I}_{in\_fn}}{G_{Net} + G_{Coil} + j\left(\omega_n C_{Net} - \frac{1}{\omega_n L_{Coil}}\right)}$$

$$= \frac{\bar{I}_{in\_fn}}{I_d + j\left(I_{cNet} \cdot \frac{\omega_n}{\omega_s} - I_{Coil} \cdot \frac{\omega_s}{\omega_n}\right)} U_{PE} \tag{48}$$

Injection current $\bar{I}_{in}$ as a function of zero-sequence voltage $\bar{U}_0$ at frequency f_n. I.e., injection current needed to obtain a certain zero-sequence voltage.

$$\bar{I}_{in\_fn} = \frac{\bar{U}_{0\_fn}(\bar{Y}_{Net}\bar{Y}_{Coil} + 3\bar{Y}_{0Tr}\bar{Y}_{Net} + 3\bar{Y}_{0Tr}\bar{Y}_{Coil})}{3\bar{Y}_{0Tr}} \tag{49}$$

Without the zero-sequence admittance $\bar{Y}_{0Tr}$.

$$\bar{I}_{in\_fn} = (\bar{Y}_{Net} + \bar{Y}_{Coil})\bar{U}_{0\_fn} \tag{50}$$

Zero-sequence voltage at coil $\bar{U}_{0Coil}$ as a function of injection current $\bar{I}_{in}$ at frequency f_n I.e., the zero-sequence voltage at coil due to injection current.

$$\bar{U}_{0Coil\_fn} = \frac{(3\bar{Y}_{0Tr} + \bar{Y}_{Net})\bar{I}_{in\_fn}}{\bar{Y}_{Net}\bar{Y}_{Coil} + 3\bar{Y}_{0Tr}\bar{Y}_{Net} + 3\bar{Y}_{0Tr}\bar{Y}_{Coil}} \tag{51}$$

Without the zero-sequence admittance $\bar{Y}_{0Tr}$.

$$\bar{U}_{0Coil\_fn} = \bar{U}_{0\_fn} = \frac{\bar{I}_{in\_fn}}{\bar{Y}_{Net} + \bar{Y}_{Coil}} \tag{52}$$

Zero-sequence impedance seen from the terminals of the injection $\bar{Z}_{inj}$ at frequency f_n.

$$\bar{Z}_{inj\_fn} = \frac{\bar{U}_{0Coil\_fn}}{\bar{I}_{in\_fn}} = \frac{3\bar{Y}_{0Tr} + \bar{Y}_{Net}}{\bar{Y}_{Net}\bar{Y}_{Coil} + 3\bar{Y}_{0Tr}\bar{Y}_{Net} + 3\bar{Y}_{0Tr}\bar{Y}_{Coil}} \tag{53}$$

Without the zero-sequence admittance $\bar{Y}_{0Tr}$.

$$\bar{Z}_{inj\_fn} = \frac{\bar{U}_{0Coil\_fn}}{\bar{I}_{in\_fn}} = \frac{1}{\bar{Y}_{Net} + \bar{Y}_{Coil}} = \frac{1}{G_{Net} + G_{Coil} + j\left(\omega_n C_{Net} - \frac{1}{\omega_n L_{Coil}}\right)} \tag{54}$$

Resonant frequency of the zero-sequence system

$$f_{res} = \frac{1}{2\pi\sqrt{LC}} = \frac{1}{2\pi\sqrt{(L_{Coil} + L_{0Tr})C_{Net}}} = f_s\sqrt{\frac{I_{Coil}}{I_{cNet}}}\sqrt{\frac{U_{PE}}{U_{PE} + I_{Coil}Z_{0Tr}/3}} \tag{55}$$

Without the inductance of the zero-sequence admittance $\bar{Y}_{0Tr}$.

$$f_{res} = \frac{1}{2\pi\sqrt{L_{Coil}C_{Net}}} = f_s\sqrt{\frac{I_{Coil}}{I_{cNet}}} \tag{56}$$

Table 4. Equations valid for voltage-controlled non-fundamental frequency injection when the injection device is modeled as a voltage source.

Zero-sequence voltage $\overline{U}_0$ as a function of injection voltage $\overline{U}_{in}$ at frequency f_n. I.e., zero-sequence voltage due to injection source voltage.

$$\overline{U}_{0\_fn} = \frac{3\overline{Y}_{0Tr}\overline{Y}_{in}}{3\overline{Y}_{0Tr}(\overline{Y}_{in} + \overline{Y}_{Coil} + \overline{Y}_{Net}) + \overline{Y}_{Net}(\overline{Y}_{in} + \overline{Y}_{Coil})}\overline{U}_{in\_fn} \tag{57}$$

Without the zero-sequence admittance $\overline{Y}_{0Tr}$.

$$\overline{U}_{0\_fn} = \frac{\overline{Y}_{in}}{\overline{Y}_{in} + \overline{Y}_{Coil} + \overline{Y}_{Net}}\overline{U}_{in\_fn} = \frac{\overline{Y}_{in}\overline{U}_{in\_fn}}{\overline{Y}_{in} + G_{Net} + G_{Coil} + j\left(\omega_n C_{Net} - \frac{1}{\omega_n L_{Coil}}\right)}$$

$$= \frac{\overline{Y}_{in}\overline{U}_{in\_fn}}{\overline{Y}_{in}U_{PE} + I_d + j\left(I_{cNet}\cdot\frac{\omega_n}{\omega_s} - I_{Coil}\cdot\frac{\omega_s}{\omega_n}\right)}U_{PE} \tag{58}$$

Injection current $\overline{I}_{in}$ as a function of the injection source voltage $\overline{U}_{in}$ at frequency f_n. I.e., injection current due to injection source voltage.

$$\overline{I}_{in\_fn} = \frac{\overline{Y}_{in}(3\overline{Y}_{0Tr}\overline{Y}_{Net} + \overline{Y}_{Coil}\overline{Y}_{Net} + 3\overline{Y}_{0Tr}\overline{Y}_{Coil})}{3\overline{Y}_{0Tr}(\overline{Y}_{in} + \overline{Y}_{Coil} + \overline{Y}_{Net}) + \overline{Y}_{Net}(\overline{Y}_{in} + \overline{Y}_{Coil})}\overline{U}_{in\_fn} \tag{59}$$

Without the zero-sequence admittance $\overline{Y}_{0Tr}$.

$$\overline{I}_{in\_fn} = \frac{\overline{Y}_{in}(\overline{Y}_{Coil} + \overline{Y}_{Net})}{\overline{Y}_{in} + \overline{Y}_{Coil} + \overline{Y}_{Net}}\overline{U}_{in\_fn} \tag{60}$$

Injection source voltage $\overline{U}_{in}$ as a function of $\overline{U}_0$ at frequency f_n. I.e., injection source voltage needed to obtain a certain zero-sequence voltage.

$$\overline{U}_{in\_fn} = \frac{3\overline{Y}_{0Tr}(\overline{Y}_{in} + \overline{Y}_{Coil} + \overline{Y}_{Net}) + \overline{Y}_{Net}(\overline{Y}_{in} + \overline{Y}_{Coil})}{3\overline{Y}_{0Tr}\overline{Y}_{in}}\overline{U}_{0\_fn} \tag{61}$$

Without the zero-sequence admittance $\overline{Y}_{0Tr}$.

$$\overline{U}_{in\_fn} = \frac{\overline{Y}_{in} + \overline{Y}_{Coil} + \overline{Y}_{Net}}{\overline{Y}_{in}}\overline{U}_{0\_fn} \tag{62}$$

Injection source voltage $\overline{U}_{in}$ as a function of injection current $\overline{I}_{in}$ at frequency f_n. I.e., injection source voltage needed to obtain a certain injection current.

$$\overline{U}_{in\_fn} = \frac{3\overline{Y}_{0Tr}(\overline{Y}_{in} + \overline{Y}_{Coil} + \overline{Y}_{Net}) + \overline{Y}_{Net}(\overline{Y}_{in} + \overline{Y}_{Coil})}{\overline{Y}_{in}(3\overline{Y}_{0Tr}\overline{Y}_{Net} + \overline{Y}_{Coil}\overline{Y}_{Net} + 3\overline{Y}_{0Tr}\overline{Y}_{Coil})}\overline{I}_{in\_fn} \tag{63}$$

Without the zero-sequence admittance $\overline{Y}_{0Tr}$.

$$\overline{U}_{in\_fn} = \frac{\overline{Y}_{in} + \overline{Y}_{Coil} + \overline{Y}_{Net}}{\overline{Y}_{in}(\overline{Y}_{Coil} + \overline{Y}_{Net})}\overline{I}_{in\_fn} \tag{64}$$

Table 5. Equations that describe the system at fundamental frequency during voltage source-based non-fundamental frequency injection.

Zero-sequence voltage $\bar{U}_0$ as a function of phase A voltage $\bar{E}_A$ during injection at the fundamental frequency f_s. I.e., the zero-sequence voltage due to asymmetry during non-fundamental frequency injection. $$\bar{U}_{0\_fs} = -\frac{\bar{Y}_{asymm}(\bar{Y}_{in} + \bar{Y}_{Coil} + 3\bar{Y}_{0Tr})}{3\bar{Y}_{0Tr}(\bar{Y}_{in} + \bar{Y}_{Coil} + \bar{Y}_{Net}) + \bar{Y}_{Net}(\bar{Y}_{in} + \bar{Y}_{Coil})}\bar{E}_A \quad (65)$$ Without the zero-sequence admittance $\bar{Y}_{0Tr}$. $$\bar{U}_{0\_fs} = -\frac{\bar{Y}_{asymm}}{\bar{Y}_{in} + \bar{Y}_{Coil} + \bar{Y}_{Net}}\bar{E}_A \quad (66)$$
Injection current $\bar{I}_{in}$ as a function of phase A voltage $\bar{E}_A$ during injection at the fundamental frequency. I.e., the leakage current through the injection device due to asymmetry during non-fundamental frequency injection. $$\bar{I}_{in\_fs} = \frac{3\bar{Y}_{0Tr}\bar{Y}_{in}\bar{Y}_{asymm}}{3\bar{Y}_{0Tr}(\bar{Y}_{in} + \bar{Y}_{Coil} + \bar{Y}_{Net}) + \bar{Y}_{Net}(\bar{Y}_{in} + \bar{Y}_{Coil})}\bar{E}_A \quad (67)$$ Without the zero-sequence admittance $\bar{Y}_{0Tr}$. $$\bar{I}_{in\_fs} = \frac{\bar{Y}_{asymm}\bar{Y}_{in}}{\bar{Y}_{in} + \bar{Y}_{Coil} + \bar{Y}_{Net}}\bar{E}_A \quad (68)$$

Based on the equation (48) in Table 3, the system's response to the current-based injection depends on the following parameters:

- The frequency f_n of the injected signal $\bar{I}_{in\_fn}$.
- The magnitude of the injected current $\bar{I}_{in\_fn}$, while the phase shift of the injected current is irrelevant.
- I_d, the magnitude of the system damping. The lower the damping, the higher the result of the injection.
- I_v, the magnitude of the system detuning. More specifically, the result of the injection depends on the difference between the network capacitive current I_{cNet} to the coil current I_{Coil} when these are scaled accordingly considering the relationship between the fundamental frequency and the injection frequency, as shown in equation (48).

The inductance of the ASC and the total network phase-to-ground capacitance create a parallel resonance circuit. Thus, based on the fundamental principle of the parallel

resonance circuit, when the injection is applied at the resonant frequency of the system, the impedance seen by the injection, i.e., the load of the injection, is limited to the real part, i.e., the resistive part, as the imaginary part of the expression is eliminated. This can be expressed as follows:

$$imag\{\bar{Z}_{inj\_fres}\} = 0, \tag{69}$$

where $\bar{Z}_{inj\_fres}$ is the impedance seen by the injection at the system's resonant frequency. Moreover, when the zero-sequence impedance of the earthing transformer is neglected, the condition of expression (69) simplifies to following form:

$$\omega_{res} C_{Net} = \frac{1}{\omega_{res} L_{Coil}}\,. \tag{70}$$

Therefore, by essentially injecting current at the resonant frequency, the effect of the system detuning that increases the power requirement of the injection is disregarded, as the load of the injection is limited to the resistive losses of the zero-sequence system, i.e., the system damping. This means that the power requirement of the injection is minimal at the resonant frequency of the system. Further, from equation (54) in Table 3, one notes that impedance seen from the terminals of the injection is highest at the resonant frequency of the system, resulting highest zero-sequence voltage response for current-based injection.

According to (56) in Table 3, the resonant frequency is determined by the ratio of the network capacitive current I_{cNet} to the coil current I_{Coil}. However, it should be noted that the actual resonant frequency of the system is given by (55) in Table 3, from which one notes that the inductive zero-sequence impedance of the earthing or main transformer $\bar{Z}_{0Tr}$ decreases the resonant frequency of the system. In addition, when the coil current I_{Coil} is increased, the latter square root term of equation (55) in Table 3 further decreases below one, thus decreasing the resonant frequency the expression gives.

Similarly, when the injection device is presented as a voltage source and a serial admittance, based on the equation (58) in Table 4, the system's response to the voltage-based fundamental frequency injection depends on the system damping I_d, system detuning I_v, and the frequency of the injected signal. In addition, based on the equation (58) in Table 4, the outcome of the voltage-based injection depends on the following parameters:

- The frequency f_n of the source voltage $\overline{U}_{in\_fn}$.
- The magnitude of the source voltage $\overline{U}_{in\_fn}$ at the frequency f_n, while the phase shift of the source voltage is irrelevant.
- $\bar{Y}_{in}$, the source admittance of the injection. The higher the source admittance (lower source impedance), the higher the outcome of the injection. The source admittance also affects the resonant frequency seen by the injection source voltage, as the source admittance is in series with the total admittance of the system.

Based on equation (68) in Table 5, the lower the source admittance, i.e., higher source impedance, results less leakage current through the injection device due to natural zero-sequence voltage. Due to the leakage current, the zero-sequence voltage at the fundamental frequency is decreased during the injection.

Finally, if distributed compensation is also considered, the total shunt admittance of the network $\bar{Y}_{Net}$ should be divided into inductive and capacitive parts, which are further scaled to the injection frequency as follows:

$$\bar{Y}_{Net} = G_{Net} + jB_{cNet} - jB_{CoilNet} = G_{Net} + j\left(\omega_n C_{Net} - \frac{1}{\omega_n L_{CoilNet}}\right). \qquad (71)$$

Therefore, it should be noted that equations (48), (54), (55), (56), and (58) in Tables 3 and 4 neglect the inductive part of the total shunt admittance of the network $\bar{B}_{CoilNet}$, thus simplifying the expressions.

5 Simulations verifying injection theory

In this chapter, the injection theory is further verified via simulations. In this thesis, the PSCAD (Power Systems Computer Aided Design) software is used to model the operation of current injection in a simplified compensated distribution network. PSCAD is designed to simulate the time domain instantaneous responses, also known as electromagnetic transients, of electrical systems. Furthermore, the PSCAD simulation data is processed and plotted using MATLAB software.

The aim of the simulations is to verify and visualize the system's response to the injection and the parameters affecting it. Further, simulations verify the validity of previously derived equations in Chapter 4 in the simulation environment. To obtain this, the simulation results are compared to the calculated outcomes given by the derived equations.

5.1 Simulation model

To simulate the system's response to the injection, a three-phase equivalent circuit of compensated distribution network with injection is implemented in PSCAD. The network is modeled essentially with respect to the zero-sequence system phenomenon since loads, line series impedances, and phase-to-phase capacitances are disregarded. The model is further kept ideal so that the simulation results are entirely comparable with the calculated results.

The main circuit of the PSCAD model is shown in Figure 21. The model comprises a single feeder representing all the feeders in the substation. It also includes a three-phase voltage source representing the main transformer, an earthing transformer with purely inductive per-phase impedance, an ASC including a power auxiliary winding (PAW) with a parallel resistor, and an operating injection device.

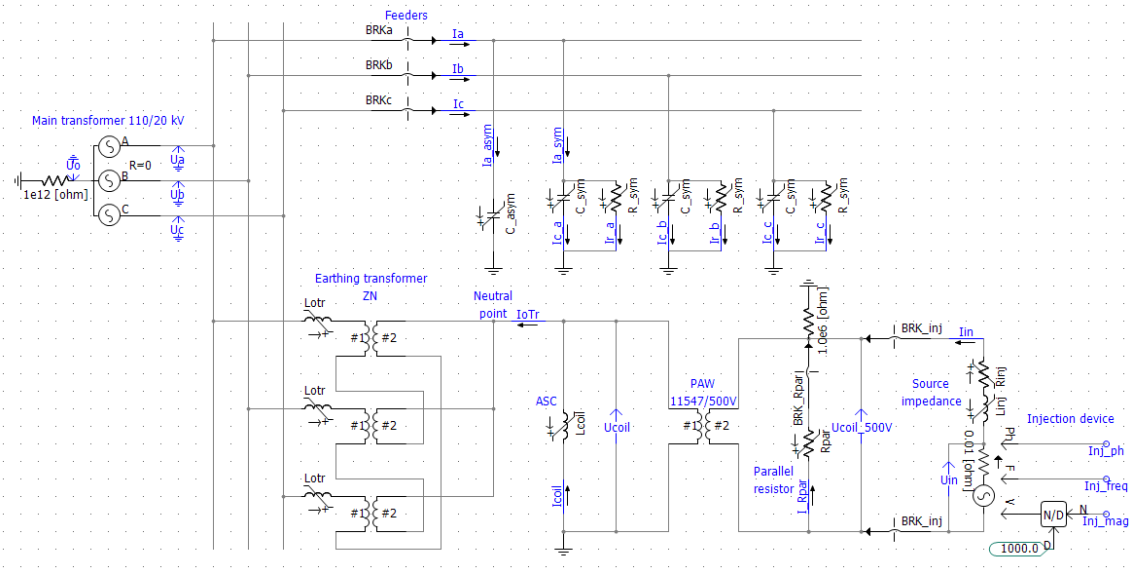

Figure 21. PSCAD model of the three-phase equivalent circuit of the compensated distribution network with current injection.

The model is parameterized with the following quantities, which are used to describe a compensated distribution network:

- f_s, the operating fundamental frequency of the system, i.e., synchronous frequency: 50 Hz.
- I_{cNet}, the capacitive earth fault current produced by the network: 20–600 A.
- I_{Coil}, the inductive current produced by the ASC. ASC tuning range: 20–600 A. Distributed compensation is not considered.
- I_d, system damping: 5–50 A, including line-to-ground losses of the feeders and parallel resistor.
- $\max(U_0)$, maximum zero-sequence voltage at resonance according to equation (18): 0–5 % of the rated phase-to-ground voltage. This parameter effectively defines the asymmetry of the network.
- Z_{0Tr}, the zero-sequence impedance of the earthing transformer: 12,3 Ω/phase. This impedance is considered to be predominantly inductive, neglecting the minor resistive component.

As given above, some parameters' values are varied and selected individually for each simulation to highlight the most relevant information. Further, all the components, e.g., transformers, voltage sources, etc., are parameterized to be ideal.

Figure 22 shows the resonance curve of the PSCAD model when the maximum zero-sequence voltage at resonance is set to 1 % of the rated phase-to-ground voltage, while the uncompensated capacitive earth fault current I_{cNet} is 100 A and system damping I_d is 15 A. It should be noted that the coil position of the ASC at resonance (peak of the resonance curve) is slightly more than 100 A due to the impedance of the grounding transformer. For the same reason, the measured zero-sequence voltage at resonance is slightly higher than 1 % of the operating nominal phase voltage, as the impedance of the grounding transformer is not considered by the equation (18).

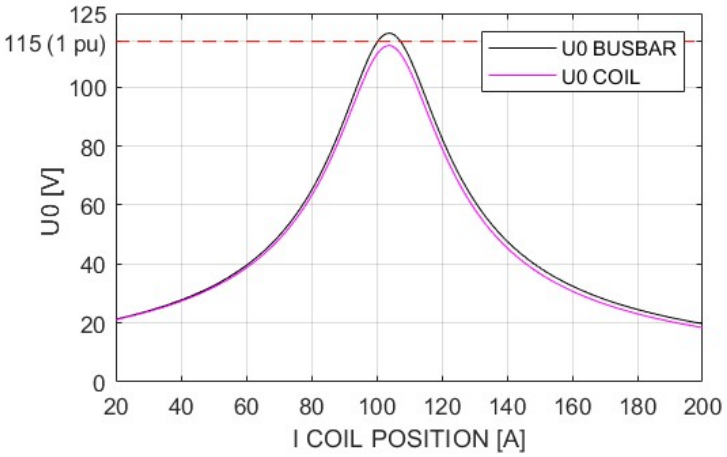

Figure 22. Example resonance curve valid for the PSCAD model.

5.2 Simulation results

This section presents simulation results from various perspectives relevant to the current injection. Specifically, it validates and visualizes the significance of different parameters that affect the system's response to the injection, including system damping and

detuning, as well as frequency and phase shift of the injection. Furthermore, the injection device is operated in current control mode, making the simulations primarily focus on current-based injections. To achieve this, the voltage source of the simulation model representing the injection device in Figure 21 is controlled so that desired current is obtained considering the magnitude, phase shift, and frequency. In addition, it should be noted that the zero-sequence voltages at coil and busbar are measured in primary, while the injection current and the impedance seen by the injection are measured in secondary.

5.2.1 Fundamental frequency injection

Based on Section 4.3.2, the system's response to the fundamental frequency injection is primarily determined by the magnitude and phase shift of the injected current and system unbalance, damping, and detuning.

5.2.1.1 The impact of the phase shift of the injection current

The impact of the phase shift of the injection current is illustrated in Figure 23, which depicts the result of the fundamental frequency injection as a function of the injection current phase shift for various system asymmetries. In Figure 23, the system is at resonance, i.e., both the uncompensated earth fault current I_{cNet} and ASC position I_{Coil} are set to 100 A in the system, while the system damping I_d is 15 A, which includes 5 A contributed by the parallel resistor.

Based on Figure 23 and as previously concluded in Chapter 4.3.2, the fundamental frequency injection can increase or decrease the natural zero-sequence voltage of the system due to asymmetry, depending on the phase shift of the injection. Correspondingly, the load, i.e., the impedance seen by the injection device, varies depending on the phase shift of the injection. However, in entirely symmetrical systems, the impact of the phase

shift of the injected current is negligible. Finally, it can be noted that the calculated results align completely with the results obtained from the simulations.

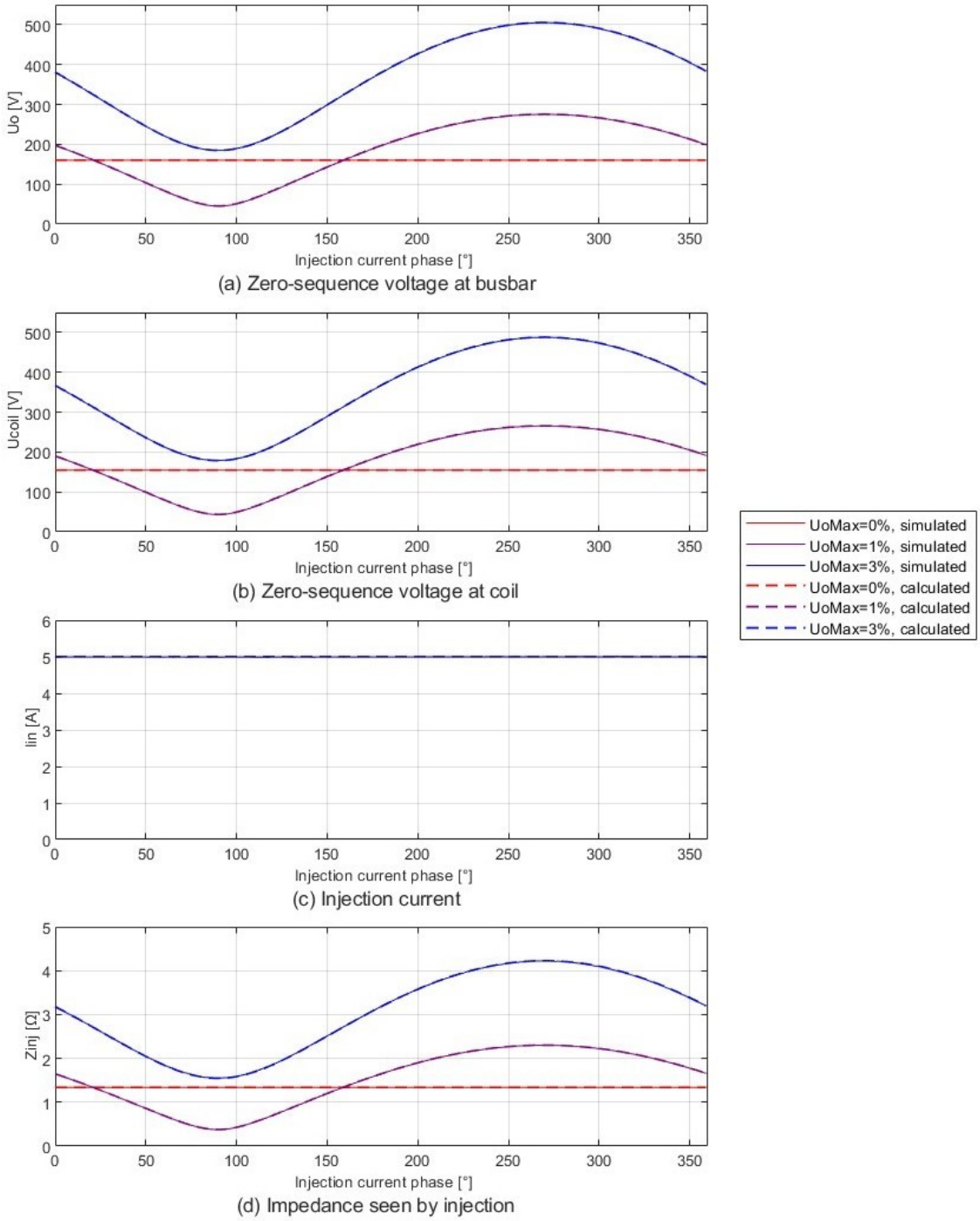

Figure 23. The impact of the phase shift of the fundamental frequency injection current for various system asymmetries.

5.2.1.2 The impact of the system damping and detuning

In Figure 24, the impact of system damping and detuning is illustrated, which shows the system's response to the fundamental frequency injection as a function of ASC current I_{Coil} for various levels of system damping I_d. The phase shift of the injected current is chosen so that the natural zero-sequence voltage of the network is increased maximally, i.e., the phase of the injected current is in phase with the zero-sequence current of the ASC. The maximum zero-sequence voltage at resonance is set to 1 % of the rated phase-to-ground voltage, while the uncompensated earth fault current I_{cNet} is 100 A in the system. The dotted line, i.e., the resonance curve, in Figure 24, describes the zero-sequence voltage prior to injection, while the solid and dashed lines illustrate the zero-sequence voltage during the injection. Thus, the change in the zero-sequence voltage due to injection can be determined.

Based on Figure 24 and as concluded in Section 4.3.2, the system's response to the fundamental frequency injection significantly decreases as the system detuning and damping are increased. When the system is at resonance, the impact of the injection is highest as the load of the injection is limited to resistive losses of the system, i.e., system damping. Predominantly, in Figure 24, the locations of the zero-sequence voltage peaks are determined by the system detuning, while the system damping determines the height and width of the peaks. Lastly, it is worth noting that the simulation outcomes align closely with the calculated results.

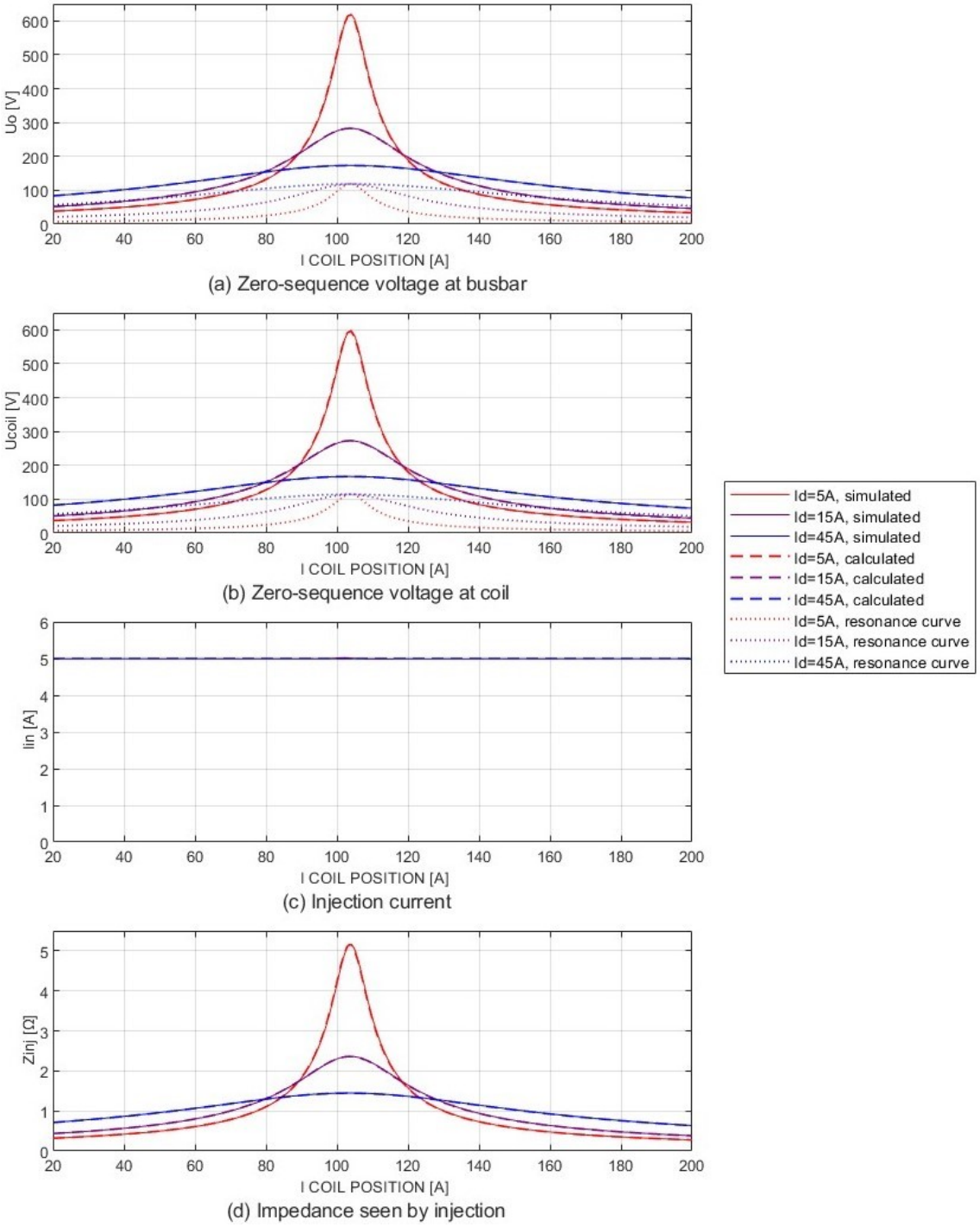

Figure 24. The impact of system detuning during fundamental frequency injection for various levels of system damping. Resonance curves are included for zero-sequence voltages at (a) and (b).

5.2.2 Non-fundamental frequency injection

Based on section 4.4.2, the system's response to the non-fundamental frequency injection is primarily determined by the magnitude and frequency of the injected current and system damping and detuning. More specifically, the outcome of the injection depends on the difference between the network capacitive current I_{cNet} and the coil current I_{Coil} when these are scaled accordingly, considering the relationship between the fundamental frequency f_s and the injection frequency f_n, as shown in equation (48) in Table 3. Furthermore, the resonant frequency is determined by the ratio of the network capacitive current I_{cNet} to the coil current I_{Coil}, as shown in equation (56) in Table 3.

5.2.2.1 The impact of the injection frequency and system detuning

In Figure 25, the system's response to the injection is illustrated as a function of ASC current I_{Coil} for various injection frequencies f_n. The uncompensated earth fault current I_{cNet} is set to 100 A, while the system damping I_d is 15 A, including the parallel resistor. The measurements are filtered so that quantities only include the components at the injection frequency. Therefore, the asymmetry of the network is irrelevant to the result of the injection.

From Figure 25, it can be observed that the location of the zero-sequence voltage response peak as a function of ASC current I_{Coil} is determined by the injection frequency f_n. Thus, by using multiple frequencies, a significant zero-sequence voltage response can be obtained over the whole ASC tuning interval. In Figures 26 and 27, this phenomenon is further illustrated from the perspective of the injection frequency.

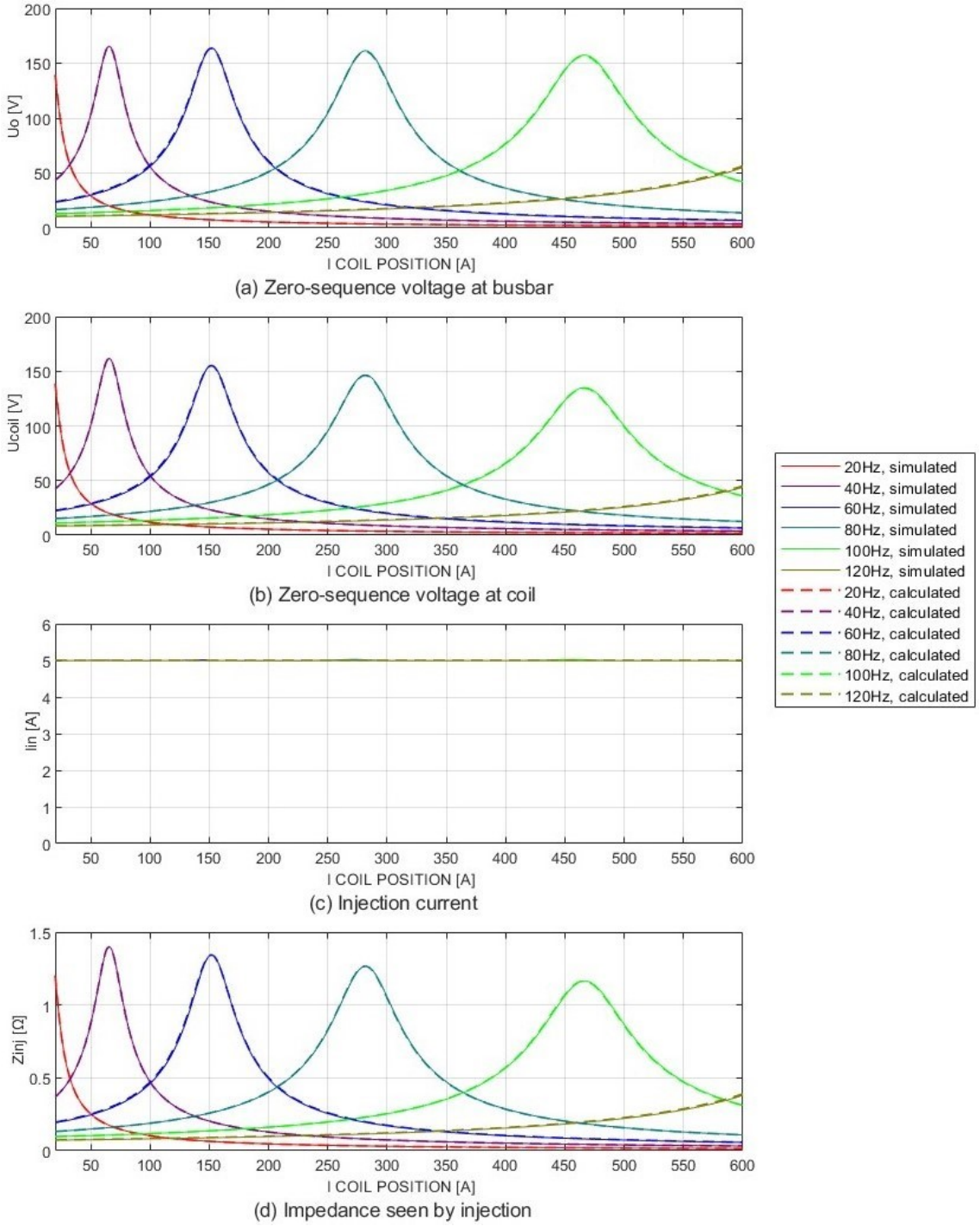

Figure 25. The impact of system detuning for various injection frequencies.

Figure 26 illustrates the system's response to the injection as a function of injection frequency f_n for various ratios of ASC current I_{Coil} to network capacitive current I_{cNet}. The uncompensated earth fault current is set to 100 A, while the ASC current varied between

20 to 600 A. However, it should be noted that the given coil tuning range is slightly unrealistic, as the typical range is from 60 to 600 A, but from the point of view of the phenomenon under study, this can be ignored. In addition, the system damping I_d is 15 A, including 5 A contributed by the parallel resistor. The network is further kept symmetric so that the outcome of 50 Hz injection is entirely comparable to other frequencies. However, the asymmetry of the network is irrelevant to the outcome of the non-fundamental frequency injection, as the measurements are filtered so that quantities only include the components at the injection frequency f_n.

Figure 26 shows that the location of the zero-sequence voltage response peaks is now determined by the ratio of network inductive current to capacitive current. The highest responses are obtained at the resonant frequency of the system given by equation (55) in Table 3. In Figure 26 (b), the peak heights of the zero-sequence voltage curves decrease as the ASC current increases. This is because as the ASC current is increased at the fundamental frequency, the impedance of the ASC is reduced. Therefore, the ASC current is also increased at the injection frequency, which leads to a larger voltage drop across the zero-sequence impedance of the earthing transformer.

Figure 27 illustrates the same phenomenon, but with the difference that now the ASC current is kept constant, while the size of the capacitive earth fault current of the network is varied. Thus, the ASC current I_{Coil} is set to 100 A, while the capacitive earth fault current I_{cNet} is varied between 20 to 600 A. Similarly to Figure 26, the network inductive current to capacitive current ratio determines the location of the zero-sequence voltage response peaks.

However, Figure 27 shows that the width of the curves decreases as the capacitive earth fault current increases. This is also true for calculated results, even though it is not obvious based on the equations that describe the system's response to injection in Table 3. Moreover, the peak heights of the curves are now equal. Although, the slight difference in peak heights is due to the frequency resolution being one hertz, which makes a

significant difference as the peaks of the curves get taper. Finally, it can also be noted that throughout this section, the outcomes of the simulations align with the calculated results.

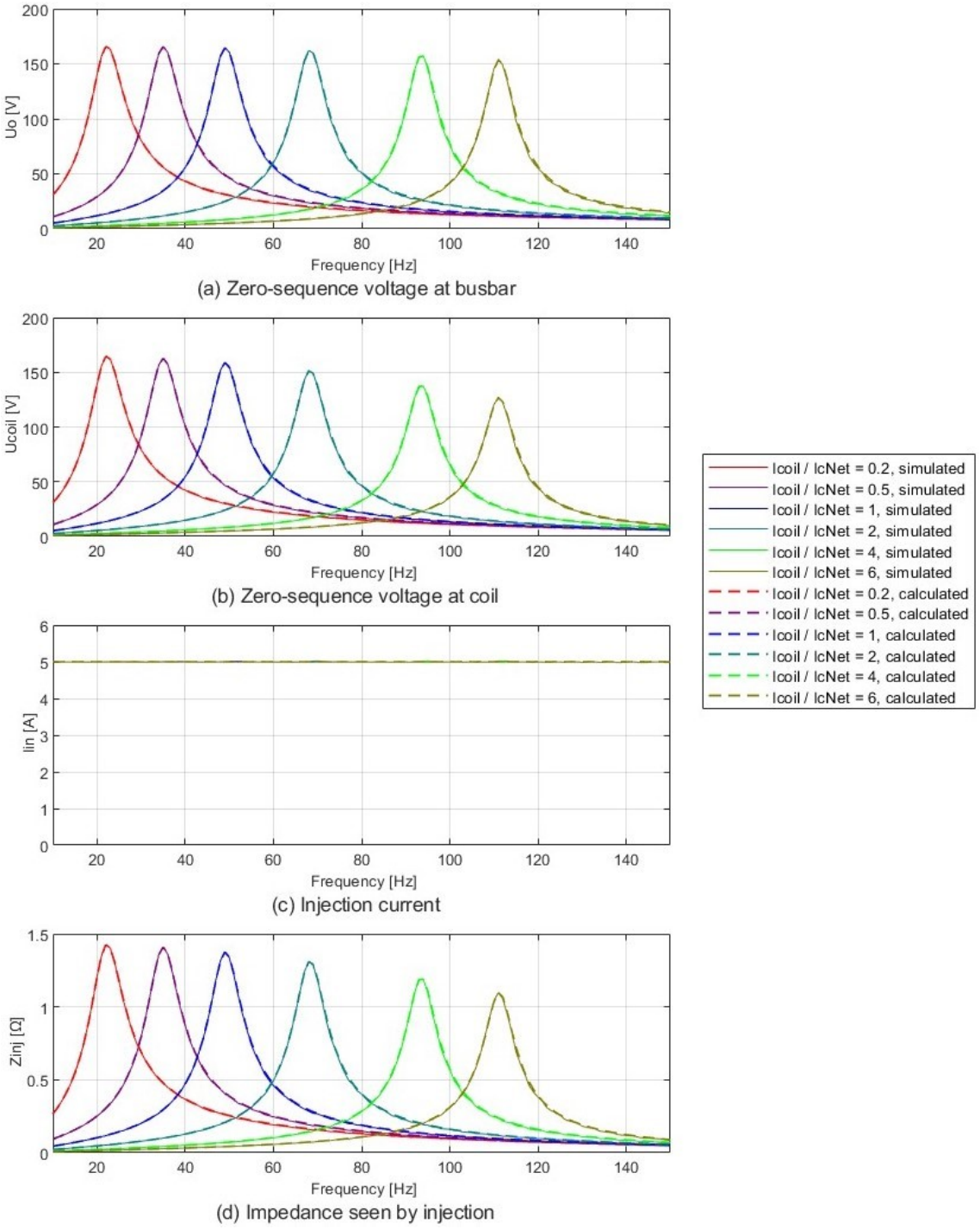

Figure 26. The impact of injection frequency for various ratios of the network inductive current to capacitive current when the inductive current is varied.

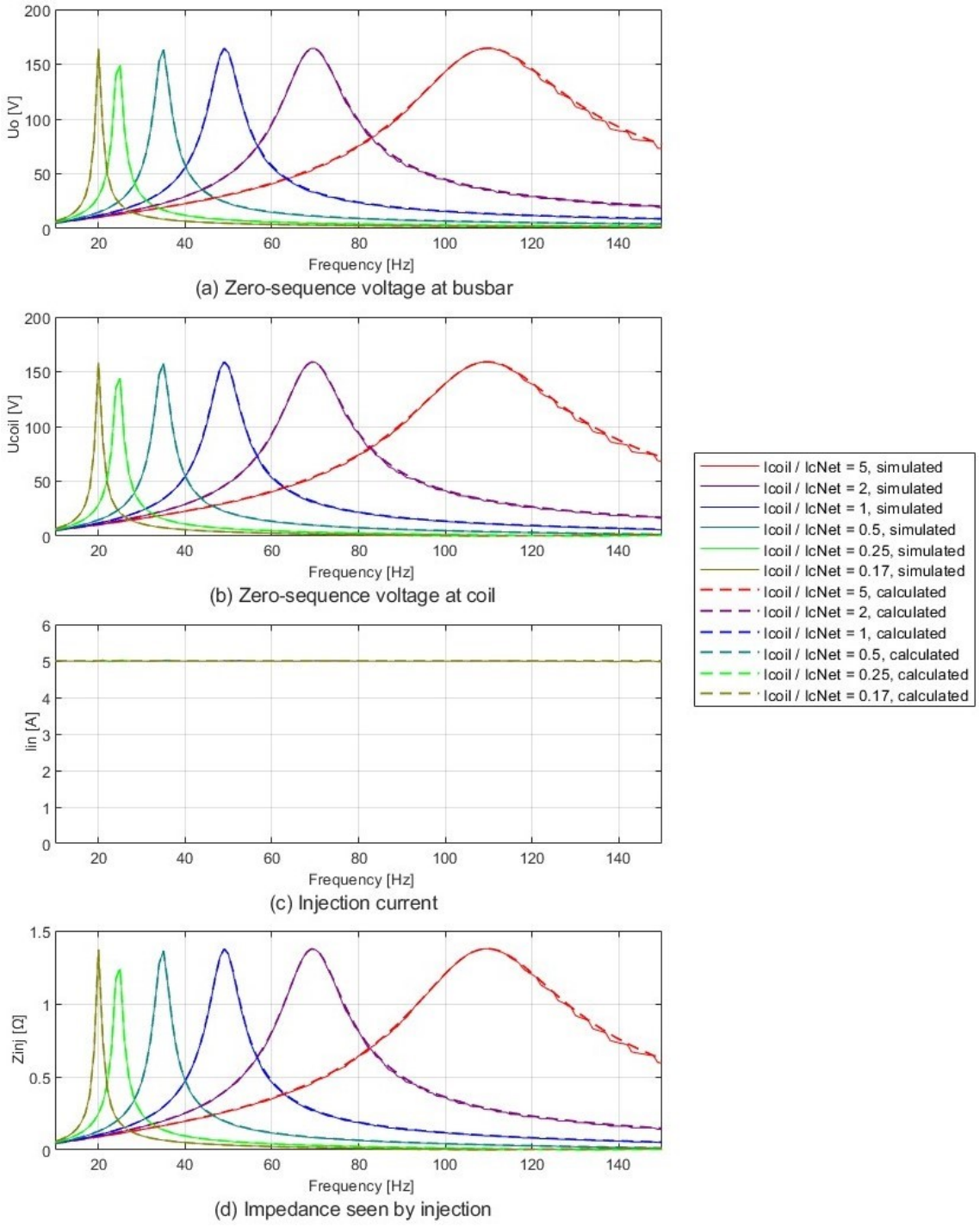

Figure 27. The impact of injection frequency for various ratios of the network inductive current to capacitive current when the capacitive current is varied.

5.2.2.2 The impact of the injection frequency and system damping

In Figure 28, the impact of the injection frequency and system damping is illustrated, which shows the system's response to the injection as a function of the injection frequency f_n for various levels of system damping I_d. The uncompensated earth fault current I_{cNet} is set to 100 A, while the ASC current I_{Coil} is 200 A. The network is further kept symmetric so that the outcome of 50 Hz injection is entirely comparable to other frequencies. However, the asymmetry of the network is irrelevant to the outcome of the non-fundamental frequency injection, as the measurements are filtered so that quantities only include the components at the injection frequency.

Based on Figure 28 and as concluded in Section 4.4.2, the system's response to the non-fundamental frequency injection is significantly decreased when the injection frequency deviates from the resonant frequency of the system. At the system's resonant frequency, the outcome of the injection is highest as the load of the injection is limited to resistive losses of the system, i.e., system damping. In addition, it should be noted that the atypical shape of the peak of the red curve in Figure 28 is because the frequency resolution is one hertz.

Furthermore, Figure 29 shows the system's response to the injection at the system's resonant frequency as a function of system damping for various injection current amplitudes. Based on Figure 29, the system's response to the injection seems to decrease according to a decreasing exponential function, which has a coefficient according to the amplitude of the injected current. As a result, when the system damping is low, the system's response to the injection is very high. Correspondingly, as the system's damping increases, the system's response to injection decreases substantially. Lastly, it is worth noting that the outcomes of the simulations align with the calculated results.

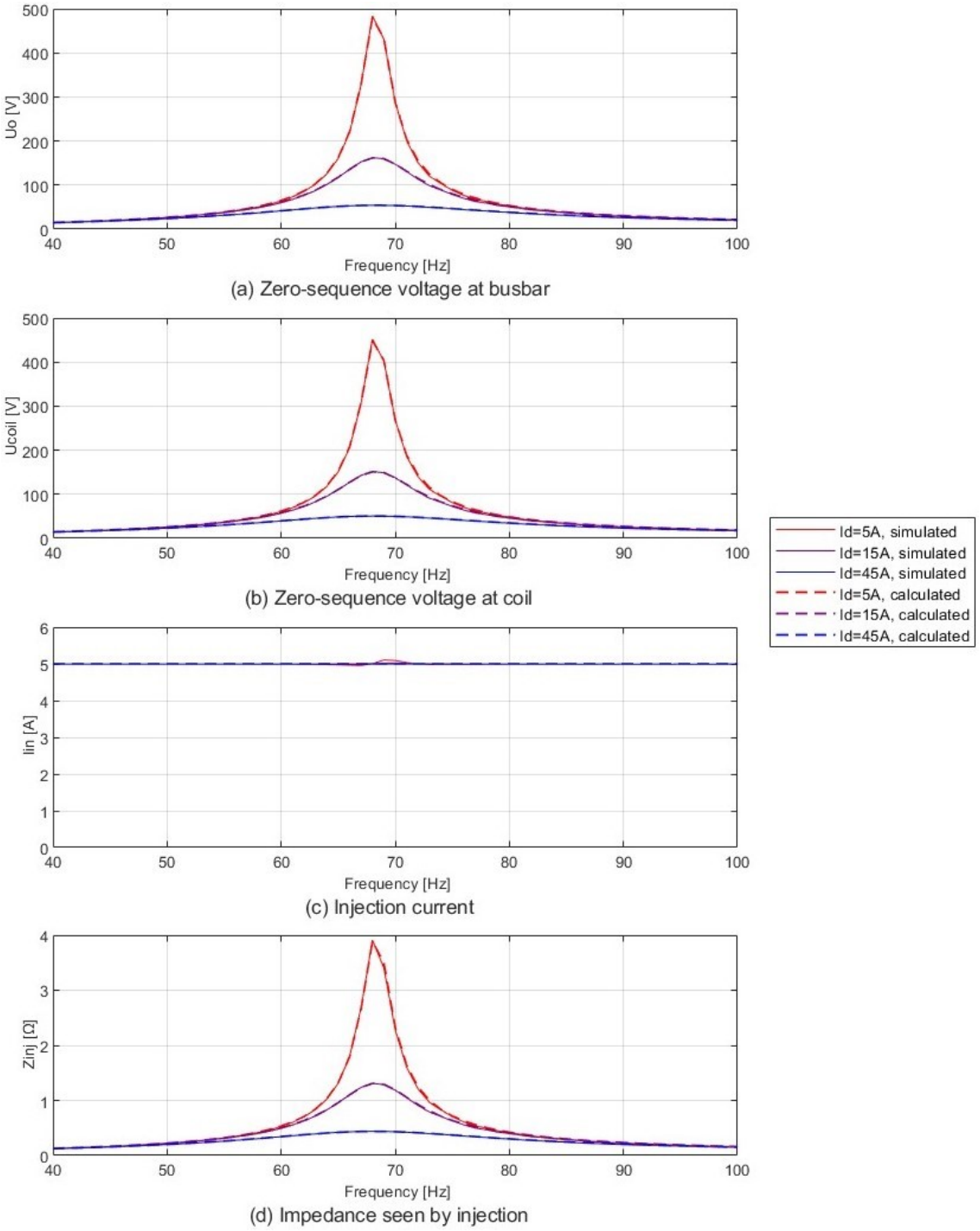

Figure 28. The impact of injection frequency for various levels of system damping.

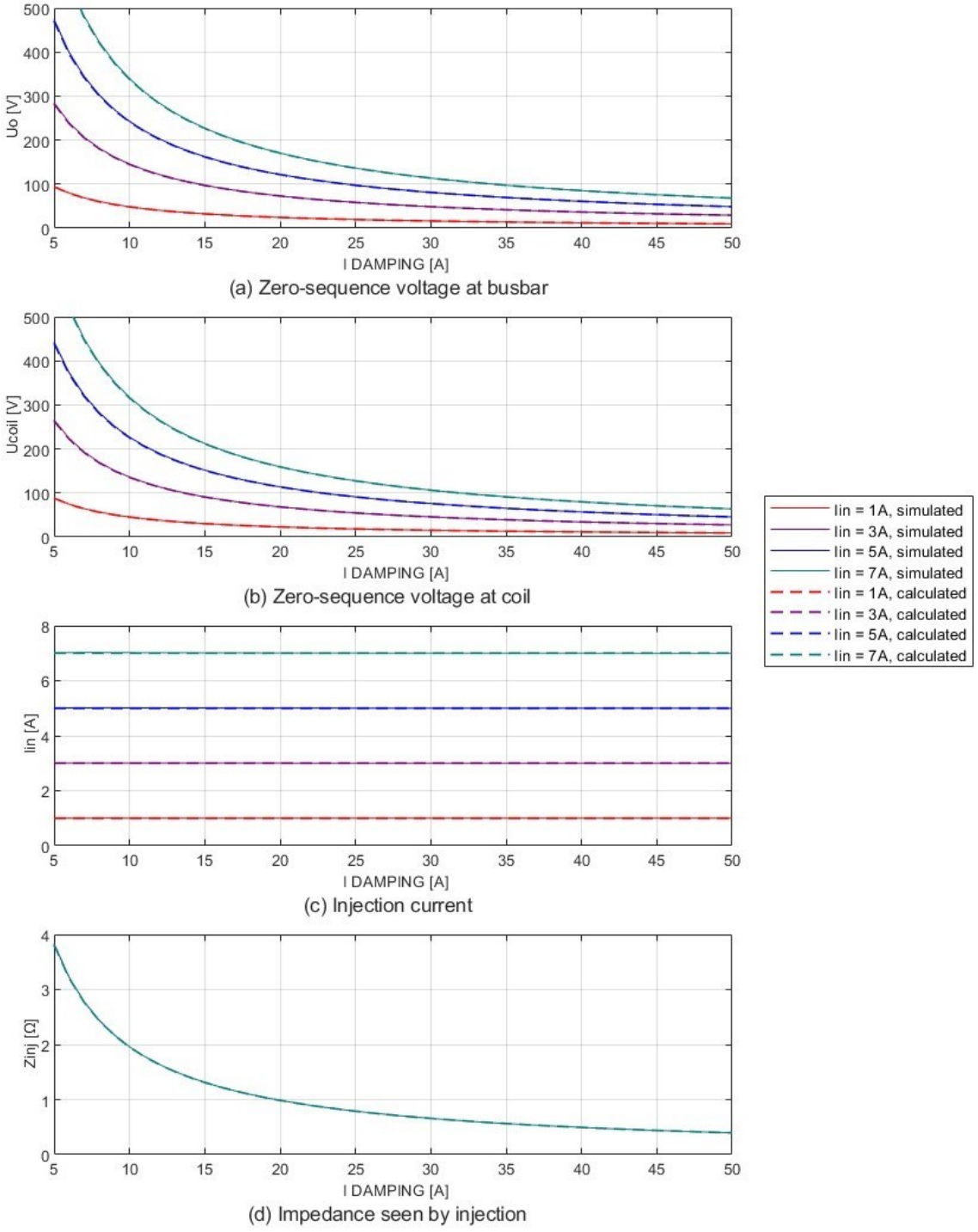

Figure 29. The impact of current injection at the resonant frequency as a function of system damping for various injection current amplitudes.

6 Arc suppression coil tuning based on active current injection

Tuning of arc suppression coil (ASC) is a major application where the current injection-based solutions are being developed and applied. The traditional ASC tuning algorithms utilize the movement of the ASC position and the natural zero-sequence voltage present in the network to determine the correct coil position, i.e., the required inductive current. The major problems for the correct calculation of the network's capacitive earth current by the traditional coil tuning methods are:

- The missing or very low zero-sequence voltage in symmetrical networks
- Crosstalk from the positive sequence system on the zero sequence system due to varying load currents (A. Eberle Gmbh & Co.KG, 2017, p. 183; Druml et al., 2005, p. 1)

The idea of the current injection is to supply alternating current to the network's zero-sequence system, thus enabling the calculation of the network's parameters or the evaluation of the state of the system detuning. Therefore, injection-based ASC tuning methods do not require sufficient natural zero-sequence voltage and can thus operate in symmetrical networks. The calculation of network parameters and the overall ASC tuning is also faster compared to traditional methods because additional coil movements are not required. However, the implementation of the current injection is more complicated and requires an additional current injection device. Moreover, implementations are manufacturer-specific.

6.1 Fundamental frequency injection

Traditionally the idea of current injection was based on injecting an artificial fundamental frequency current into the neutral point of the system if the natural zero-sequence voltage is missing or is very low, i.e., the network is symmetrical (Drum et al., 2005, p. 2). However, in asymmetrical networks, the phase shift of the injected current becomes a

critical factor to consider. One option is to supply the injected current in different phase shifts to achieve the desired response. The influence of the natural asymmetry can also be partly compensated using a differential measurement from two time points, before and after injection (Drum et al., 2005, p. 2). Thus, the following equation, combined with the coil position, enables determining the uncompensated capacitive earth fault current and the total zero-sequence losses of the network:

$$\overline{Y}_{inj} = \frac{d\overline{I}_{in}}{d\overline{U}_0} \approx G_{0Tot} + j(B_{EFNet} - B_{Coil}), \tag{72}$$

where $\overline{Y}_{inj}$ is the admittance seen by the injection, i.e, zero-sequence admittance of the system, $d\overline{I}_{in}$ is the differential of injected current, $d\overline{U}_0$ is the differential of zero-sequence voltage, and G_{0Tot} is the total zero-sequence conductance of the system (Drum et al., 2005, p. 2; Trench Austria GmbH, 2003, p. 65). Additionally, using multiple injection cycles, typically 2 or 3, with varying amplitudes or phase shifts, the inductance of the ASC and system asymmetry can also be solved.

The Earth-fault compensation controller, EFC60s (previously EFC50i), by Trench Group (2013 p. 3; 2021b, p. 3) incorporates a separate current injection device ECI for single frequency 50 or 60 Hz current injection. The current injection device ECI consists of a transformer and capacitors for current limiting (Trench Group, 2013, p. 8). The EFC60s calculates the resonance curve by injecting a current into the network's zero-sequence system and measuring the phasors of the zero-sequence voltage and the injected current (Trench Group, p. 4). The controller also allows a permanent current injection to raise the low natural zero-sequence voltage.

The fundamental frequency injection still has the disadvantage that the calculation accuracy suffers due to the fundamental frequency disturbances. A simple stability validation is to compare the zero-sequence voltage before and after the measurement (Schlömmer et al., 2017, p. 2). Further improvement can also be attained by extending

the measurement intervals, thus allowing for better averaging of interferences and minimizing their impact.

Furthermore, achieving a sufficient zero-sequence voltage response to injection is crucial to accurately estimating the network parameters. However, as the system detuning increases, the system's response to fundamental frequency injection significantly decreases. If used over the entire ASC tuning interval in severe detunings, this poses a significant power requirement for the injection device.

6.2 Injection of two frequencies

Due to the weaknesses of the fundamental frequency injection, the next evolution in injection-based coil tuning methods was the injection of two frequencies different from the fundamental frequency of the system. Although, it should be noted that the injection signal in this method contains multiple frequencies, contrary to the description that implies the injection of only two frequencies (A. Eberle Gmbh & Co.KG, 2017, pp. 189–191; Trench Group, p. 3). However, the method calculates network parameters using only the two most dominant frequencies.

The method was first introduced by A. Eberle Gmbh & Co.KG and subsequently also adopted by Trench Group (Druml et al., 2005; Schlömmer et al., 2017; Trench Group, p. 3). The corresponding commercial products of the previous vendors are CI (Current Injection for Low or Highly Variable Zero-Sequence Voltages) and the current injection device ECI, respectively. Further, the petersen coil regulator REG-DPF, operates as a control unit for the CI (A. Eberle Gmbh & Co.KG, 2017). Similarly, the ECI is controlled by the earth-fault compensation controller EFC60m (Trench Group, 2021a).

The current signal containing non-fundamental frequencies can be generated by pulsing a 50 Hz injection signal over some limiting impedance using the arrangement shown in

Figure 30 (A. Eberle Gmbh & Co.KG, 2017, p. 189; Druml et al., 2005, pp. 3–4; Schlömmer et al., 2017, pp. 2–3). Figure 31 illustrates the waveform of the resulting signal, for which the frequency spectrum is shown in Figure 32. The network parameters are then calculated using the two highest non-fundamental frequencies, 42 and 58 Hz (A. Eberle Gmbh & Co.KG, 2017, p. 189). However, the main disadvantage of this current injection type is that the most significant frequency component is 50 Hz, thus unnecessarily increasing the power requirement.

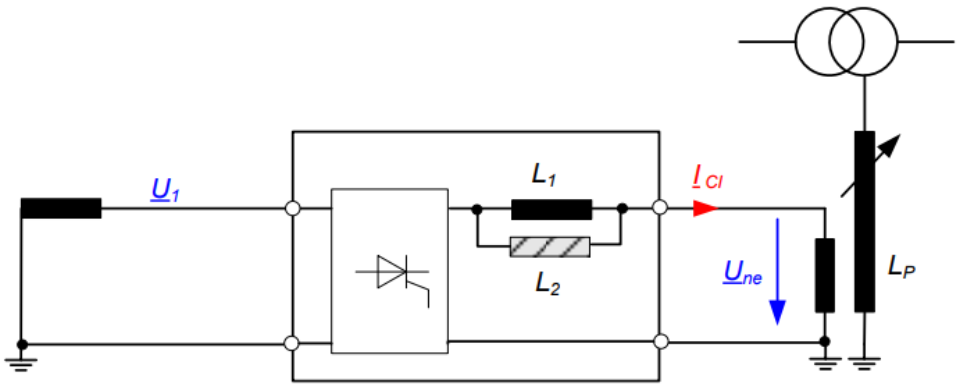

Figure 30. Simplified current injection diagram with three frequencies (A. Eberle Gmbh & Co.KG, 2017, p. 189).

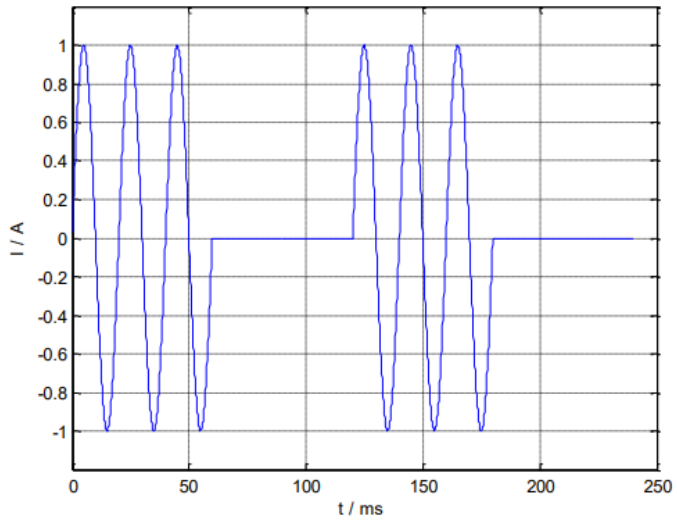

Figure 31. Example for the pulse pattern for injection with 50 Hz component (A. Eberle Gmbh & Co.KG, 2017, p. 189).

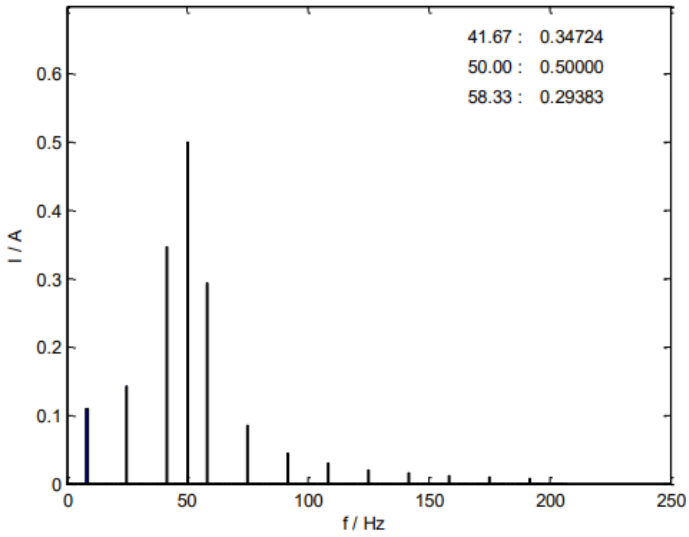

Figure 32. Frequency spectrum for injection with 50 Hz component (A. Eberle Gmbh & Co.KG, 2017, p. 189).

Further improvement is obtained by alternating switching of both polarities of the fundamental frequency (Druml et al., 2005, p. 4). This can be implemented using the arrangement shown in Figure 33, where it is possible to invert the direction of the current. Figure 34 illustrates the waveform of the resulting signal, for which the frequency spectrum is shown in Figure 35.

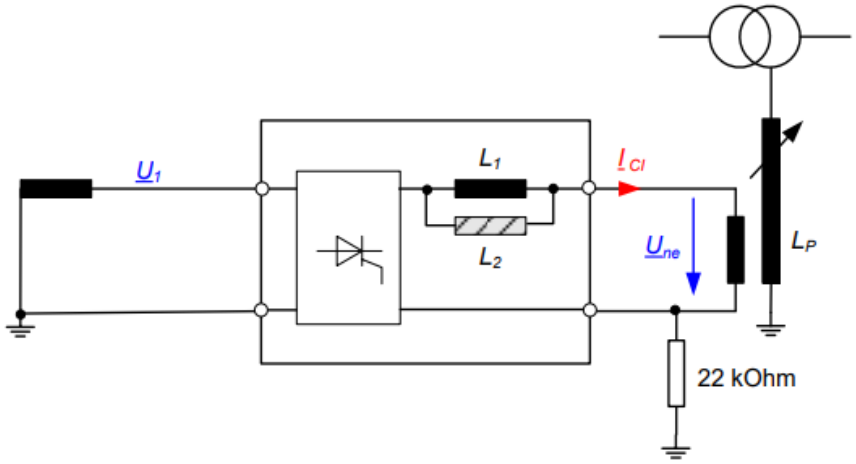

Figure 33. Simplified current injection diagram with only two frequencies without 50 Hz (A. Eberle Gmbh & Co.KG, 2017, p. 190).

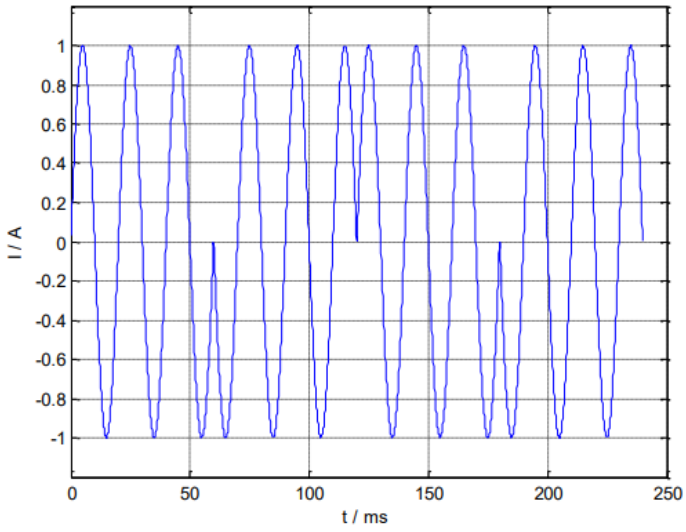

Figure 34. Example for the pulse pattern for injection without 50 Hz component (A. Eberle Gmbh & Co.KG, 2017, p. 190).

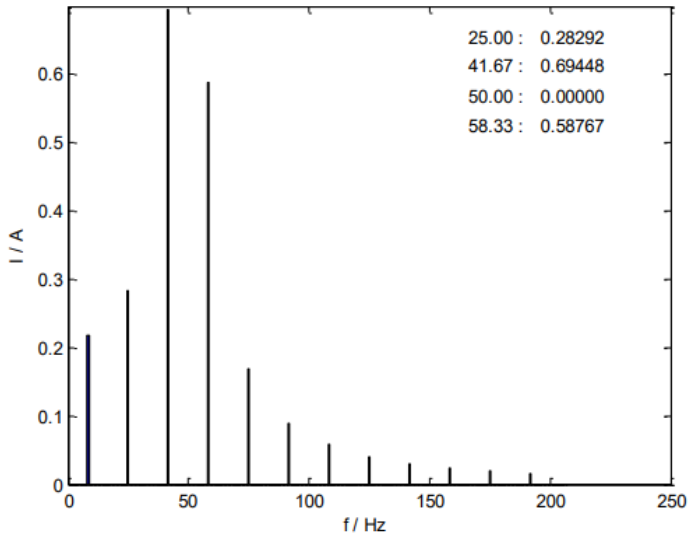

Figure 35. Frequency spectrum for injection without 50 Hz component (A. Eberle Gmbh & Co.KG, 2017, p. 191).

It is also mentioned that the amplitude of the injected current should be variable to adjust to the system damping in different switching states (A. Eberle Gmbh & Co.KG, 2017, p. 185). This is because the current injection can lead to undesirably strong influences on the zero-sequence voltage, so the earth fault threshold may be exceeded. On the other hand, in situations with high detuning, a lower injected current will not deliver a reliable measurement of the zero-sequence voltage (Druml et al., 2005, p. 3). The reduced current injection is achieved through phase angle control, as illustrated in Figure 36.

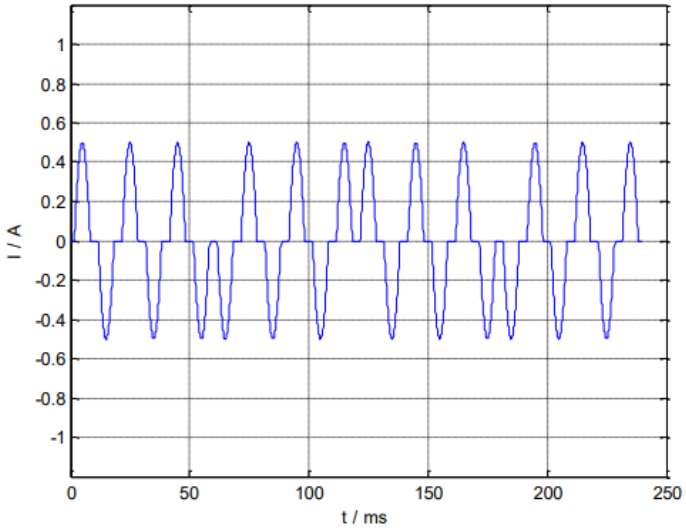

Figure 36. Example for a pulse pattern with reduced power (A. Eberle Gmbh & Co.KG, 2017, p. 191).

However, despite the improvements, Vancata and Matuljak (2019, pp. 1–2) listed the following drawbacks of the method described in this section:

- A true current source is not used. Instead, a thyristor-switched voltage source is used to generate the injected signal. As a result, the injected current value depends on the magnitude and phase shift of the natural zero-sequence voltage.
- As the evaluated frequencies are close to the fundamental frequency, the system's response to injection decreases rapidly as the system detuning increases.
- The amplitudes of the produced side frequency components are considerably attenuated when the frequency difference to the fundamental frequency increases.

Despite the previous drawbacks, based on the early operational field experience presented by Druml et al. (2007, pp. 3–4), the described method had no problems finding the correct operation point, and the tuning succeeded even in networks with low or high natural zero-sequence voltage and high crosstalk from load current.

6.2.1 CIF algorithm for parameter estimation

A. Eberle Gmbh's (2017, pp. 183–184) CIF algorithm (Control by Injecting Frequencies) of the REG-DPA Petersen coil regulator calculates the network parameters using the two injected frequencies unequal to 50 Hz. The tuning is initiated after detecting a relative change in zero-sequence voltage caused by a switching operation (Druml et al., 2005, p.3). However, if the natural zero-sequence voltage is very low, a cyclic calculation enables checking the network parameters at regular intervals, e.g., every 60 min (A. Eberle Gmbh & Co.KG, 2017, p. 200).

The parameter estimation using the injection of two frequencies can be derived from the equivalent circuit shown in Figure 37, which is an alternative to the equivalent circuit presented in Figure 17.

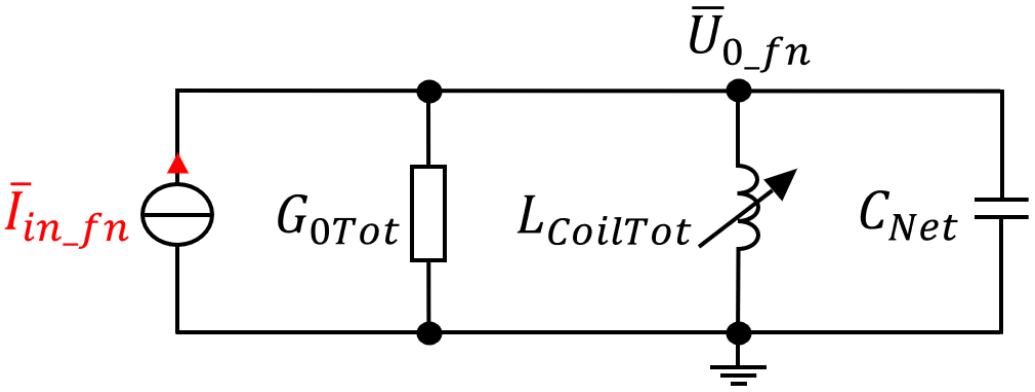

Figure 37. Simplified one-phase equivalent circuit with current injection unequal to 50 Hz.

The system's zero-sequence admittance seen by the injection can be formulated for the current injection as follows:

$$\overline{Y}_{inj\_fn} = \frac{\overline{I}_{in\_fn}}{\overline{U}_{0\_fn}} = G_{0Tot} + j\left(\omega_n C_{Net} - \frac{1}{\omega_n L_{CoilTot}}\right), \tag{73}$$

where $L_{CoilTot}$ is the inductance of all connected ASCs, including distributed compensation, and $\overline{Y}_{inj\_fn}$ is the admittance seen by the injection, i.e., the zero-sequence admittance of the system at frequency f_n (A. Eberle Gmbh & Co.KG, 2017, p. 184). When two frequencies f_1 and f_2 are used, two complex equations with three variables are created, which leads to the following solution:

$$G_{0Tot} = real\{\overline{Y}_{inj\_f1}\} = real\{\overline{Y}_{inj\_f2}\}, \tag{74}$$

$$C_{Net} = \frac{imag\{\overline{Y}_{inj\_f1}\}\omega_1 - imag\{\overline{Y}_{inj\_f2}\}\omega_2}{\omega_1^2 - \omega_2^2}, \tag{75}$$

$$L_{CoilTot} = \frac{\omega_1^2 - \omega_2^2}{imag\{\overline{Y}_{inj\_f1}\}\omega_1\omega_2^2 - imag\{\overline{Y}_{inj\_f2}\}\omega_2\omega_1^2}, \tag{76}$$

where $\overline{Y}_{inj\_f1}$ and $\overline{Y}_{inj\_f2}$ are the zero-sequence admittances of the system at angular frequencies ω_1 and ω_1 (Talla et al., 2016, p. 388). Alternatively, $L_{CoilTot}$ can be expressed in terms of C_{Net} as follows:

$$L_{CoilTot} = \frac{1}{-imag\{\overline{Y}_{inj\_f1}\}\omega_1 + \omega_1^2 C_{Net}}. \tag{77}$$

The system detuning at fundamental frequency in amperes can then be determined as follows by taking into account the positive sequence voltage U_{PE}:

$$I_v = U_{PE}\left(\frac{1}{\omega_s L_{CoilTot}} - \omega_s C_{Net}\right). \tag{78}$$

More information on the practical realization of the method, including system measurement points, is addressed in (A. Eberle Gmbh & Co.KG, 2017, pp. 193–195; Druml et al., 2007, pp. 2–3).

6.2.2 More precise models

More accurate results can be obtained using more precise models that do not neglect the zero-sequence impedance of the earthing or main transformer. For this reason, the CIF algorithm also enables to measure the zero-sequence impedance of the transformer by measuring the zero-sequence current of the transformer and zero-sequence voltages at the coil and busbar (Druml et al., 2005, p. 5). More precise models are further briefly discussed in (Druml et al., 2005, pp. 4–5; Druml & Seifert, 2005, pp. 4–5).

A method determining network parameters with non-negligible zero-sequence admittance of the transformer is described in the patent by Druml and Kugi (2005). The following equivalent circuit in Figure 38 is adapted to describe the method.

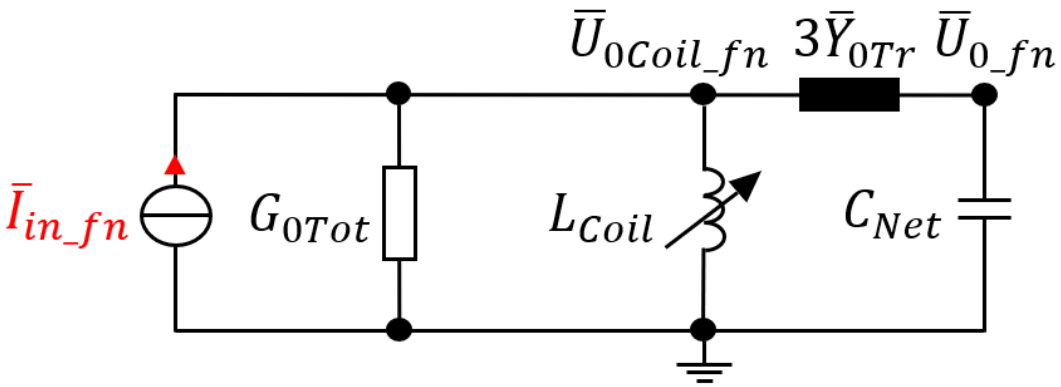

Figure 38. Simplified one-phase equivalent circuit with non-negligible zero-sequence admittance of the zero transformer and current injection unequal to 50 Hz.

The method establishes the following relation by measuring the zero-sequence voltage at coil and busbar:

$$K_{fn} = \frac{\overline{U}_{0Coil\_fn}}{\overline{U}_{0\_fn}} = \frac{\frac{1}{j\omega_n C_{Net}} + j\omega_n L_{0Tr}}{\frac{1}{j\omega_n C_{Net}}} = \frac{\frac{1}{\omega_n C_{Net}} - \omega_n L_{0Tr}}{\frac{1}{\omega_n C_{Net}}}$$
$$= 1 - \omega_n^2 L_{0Tr} C_{Net}, \tag{79}$$

where K_{fn} is the ratio between the zero-sequence voltage phasors measured at coil and busbar and L_{0Tr} is the zero-sequence inductance of the transformer. The system's zero-sequence admittance seen by the injection now has the following form:

$$\overline{Y}_{inj\_fn} = \frac{\overline{I}_{in\_fn}}{\overline{U}_{0Coil\_fn}} = G_{0Tot} + \frac{1}{j\omega_n L_{Coil}} + \frac{1}{j\omega_n L_{0Tr} + \frac{1}{j\omega_n C_{Net}}}. \tag{80}$$

The imaginary part of the previous admittance can then be expressed by using the ratio K_{fn} as follows:

$$B_{inj\_fn} = imag\left\{\frac{\overline{I}_{in\_fn}}{\overline{U}_{0Coil\_fn}}\right\} = -\frac{1}{\omega_n L_{Coil}} + \frac{\omega_n C_{Net}}{K_{fn}}, \tag{81}$$

where B_{inj_fn} is the system's zero-sequence susceptance seen by the injection. Then for two frequencies f_1 and f_2 unequal to 50 Hz, the corresponding zero-sequence admittances B_{inj_f1} and B_{inj_fn} can be calcultated. This creates two equations that provide the following solution:

$$L_{Coil} = \frac{K_{f2}\omega_1^2 - K_{f1}\omega_2^2}{\omega_1\omega_2\left(B_{inj\_f1}\omega_2 K_{f1} - B_{inj\_f2}\omega_1 K_{f2}\right)}, \tag{82}$$

$$C_{Net} = \frac{K_{f1}K_{f2}\left(B_{inj\_f1}\omega_1 - B_{inj\_f2}\omega_2\right)}{K_{f2}\omega_1^2 - K_{f1}\omega_2^2} = \frac{K_{f1} + B_{inj\_f1}\omega_1 L_{Coil}K_{f1}}{\omega_1^2 L_{Coil}}. \tag{83}$$

Finally, the system detuning at the fundamental frequency in amperes can be calculated as follows:

$$I_v = U_{PE}\left(\frac{1}{\omega_s(L_{Coil} + L_{0Tr})} - \omega_s C_{Net}\right). \tag{84}$$

6.3 Multi-frequency current injection

This section describes the operation of the commercial product Multi-Frequency Current Injector (MCI) developed by the combined efforts of the two leading manufacturers A. Eberle Gmbh and EGE, spol. s r.o. The MCI is currently the most advanced injection-based solution in the market for ASC tuning. Especially, the weaknesses of the previous method discussed in Section 6.2 have been considered in the MCI development.

The MCI utilizes a semiconductor frequency converter to generate a multifrequency current signal consisting of eight different frequency components of equal amplitude of 2,5 A ranging from 15–160 Hz, resulting a total RMS current value of 5 A (EGE spol. s r.o., 2020, p. 2; Vancata et al., 2021, p. 2). Figure 39 illustrates a waveform of such a signal, for which the frequency spectrum is shown in Figure 40.

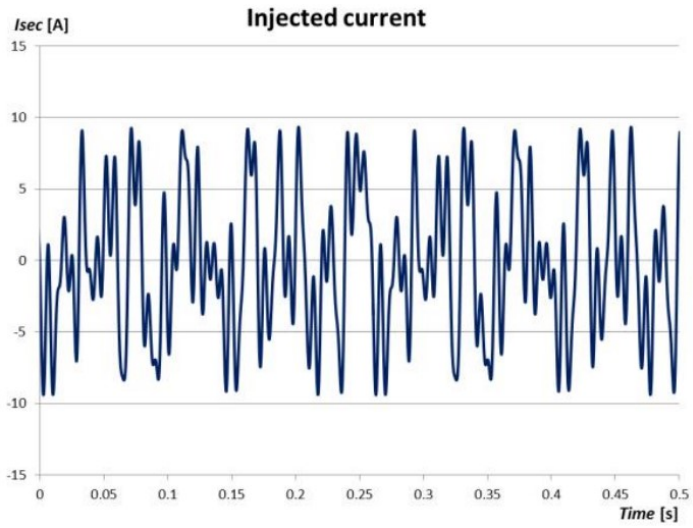

Figure 39. Optimized multifrequency current signal (Vancata & Matuljak, 2019, p. 3).

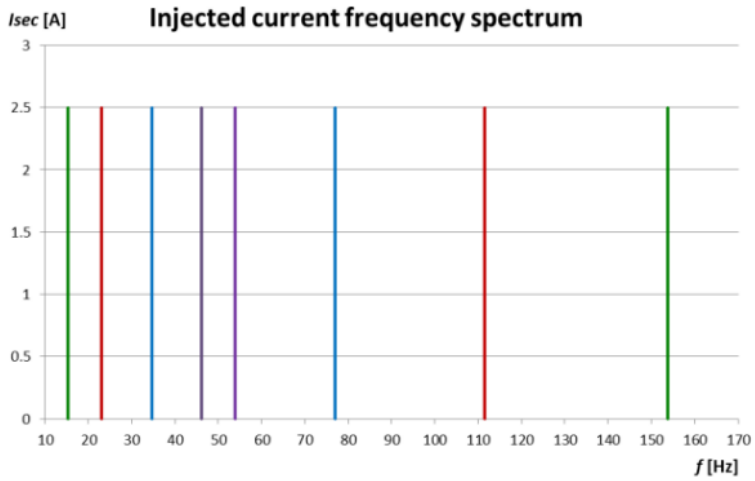

Figure 40. Frequency spectrum of a truly multifrequency current signal (Vancata & Matuljak, 2019, p. 2).

The 15–160 Hz frequency range corresponds to the typical resonant frequencies of the network's zero-sequence system. More specifically, using the approximation equation (56) in Table 3 to calculate the resonant frequency, it is found that the frequency range limits f_{1ow} and f_{high} correspond to the following under-compensated and over-compensated situations where the inductive current is one-tenth or ten times the network capacitive current:

$$f_{1ow} = 50\ Hz \sqrt{\frac{I_{Coil}}{I_{cNet}}} = 50\ Hz \sqrt{\frac{0{,}1 \cdot I_{cNet}}{I_{cNet}}} = 50\ Hz \sqrt{0{,}1} = 15{,}8\ Hz, \tag{85}$$

$$f_{high} = 50\ Hz \sqrt{\frac{I_{Coil}}{I_{cNet}}} = 50\ Hz \sqrt{\frac{10 \cdot I_{cNet}}{I_{cNet}}} = 50\ Hz \sqrt{10} = 158\ Hz. \tag{86}$$

The idea of using the wide frequency range is to ensure that the zero-sequence voltage response is high enough in the whole ASC tuning interval, even in extremely detuned situations (see section 5.2.2.1.). This is illustrated in Figure 41, which shows the zero-sequence voltage responses for the different frequency components of the current signal shown in Figure 40.

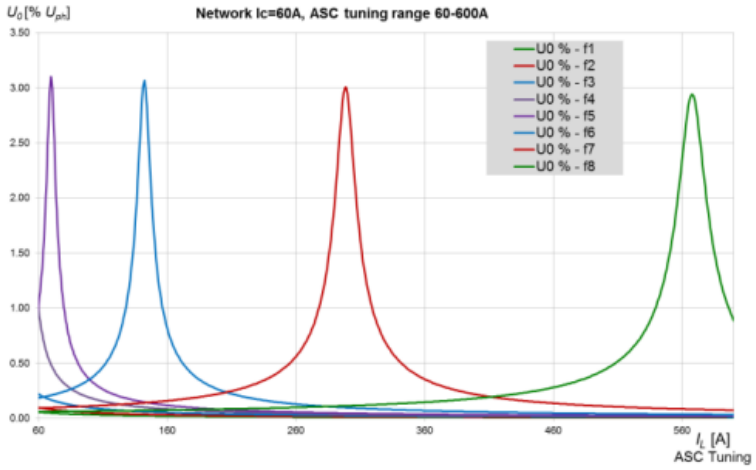

Figure 41. Voltage response for all the frequency components in zero sequence system in case of over-tuned ASC (Vancata & Matuljak, 2019, p. 2).

Due to the wide frequency range, injecting unnecessarily high currents can be avoided, thus allowing reduced power and dimensions. However, the power is still sufficient even for large and very damped networks (Vancata et al., 2021, pp. 1–2). Despite the aforementioned facts, it should be noted that injecting multiple frequencies at the same time increases the power and computational demands for results evaluation (Talla et al., 2016, p. 388). Although, the absolute current amplitude can be minimized by phase shift optimization between the frequency components, as illustrated in Figure 39, where the current amplitude remains under 10 A (Talla et al., 2016, p. 388–389; Vancata & Matuljak, 2019, p. 3).

According to the datasheet, the MCI can operate in 20 kV networks with average damping up to 1300 A of capacitive earth fault current (A. Eberle Gmbh & Co.KG, 2020, p. 3). However, the current injection can lead to undesirably strong influences on the zero-sequence voltage, especially at the resonant frequency. To prevent this, the MCI has a power reduction functionality that monitors the influence of the zero-sequence voltage (A. Eberle Gmbh & Co.KG, 2023).

The MCI also allows for continuous current injection and real-time calculation of network parameters during the tuning process (Vancata et al., 2021, p. 2). In contrast, previous methods calculate network parameters only before and after the coil movements, often requiring additional iteration steps for coil tuning. With the new method, the need for these extra steps is eliminated as the network parameter calculations are continuously updated throughout the tuning process.

In the early operational testing, the MCI was found to be reliable in many situations that are challenging for traditional coil tuning methods, such as in symmetrical networks and in situations where the zero-sequence voltage of the network is unstable (Vancata et al., 2021, pp. 3–5). The MCI could reliably determine the network parameters even when the position of the coil is extremely under-compensated or over-compensated due to the wide frequency range of the injected signal (Vancata et al., 2021, pp. 2–3). In the laboratory testing, the calculation was accurate enough regardless of the variation in system damping, ranging from 1,5 to 60 A (Vancata et al., 2021, p. 3).

6.3.1 Complementary frequencies

The injected frequencies can be selected so that the frequency spectrum consists of pairs of complementary frequencies defined by the following equation:

$$f_i \cdot f_{ii} = f_s^2, \tag{87}$$

where f_i and f_{ii} are the frequencies of the complementary frequency pair (Vancata & Matuljak, 2019, p. 3). In this case, the zero-sequence voltage amplitude response for a complementary frequency pair can be used to determine whether the system is under-compensated or over-compensated, or at resonance (Matuljak & Vancata, 2016, pp. 26–27; Vancata & Matuljak, 2019, p. 3). One of the complementary frequencies f_i used for the tuning process can preferably be the resonant frequency f_{res} of the system, in which

case the most accurate results are achieved for setting the ASC (Matuljak & Vancata, 2016, pp. 10, 18–19, 28).

A major benefit of using complementary frequencies is that it allows simpler calculation of network parameters compared to non-complementary frequencies (Vancata & Matuljak, 2019, pp. 3–4). For each pair of complementary frequencies ω_i and ω_{ii}, the zero-sequence admittances of the system, $\overline{Y}_{inj\_fi}$ and $\overline{Y}_{inj\_fii}$, can be calculated as illustrated in Section 6.2.1. Then the system detuning at the fundamental frequency can be solved remarkably simply using the imaginary parts, B_{inj_fi} and B_{inj_fi}, of the previous admittances as follows:

$$\begin{aligned}\Delta B_s &= B_{cNet} - B_{CoilTot} = \omega_s C_{Net} - \frac{1}{\omega_s L_{CoilTot}} \\ &= \frac{\omega_s}{\omega_i + \omega_{ii}}\left(B_{inj\_fi} + B_{inj\_fii}\right),\end{aligned} \tag{88}$$

where ΔB_s is system detuning in terms of susceptance at the fundamental frequency, $B_{CoilTot}$ is the inductive susceptance of all connected ASCs, including distributed compensation (Matuljak & Vancata, 2016, p. 20; Vancata & Matuljak, 2019, p. 4). The system detuning in amperes at the fundamental frequency can then be calculated as follows:

$$I_v = -\Delta B_s \cdot U_{PE}, \tag{89}$$

Also, the phase-to-ground capacitance of the network and the inductance of all the connected ASCs, including distributed compensation, can be calculated as follows:

$$C_{Net} = \frac{\omega_{ii}\Delta B_s - \omega_s B_{inj\_fi}}{\omega_s(\omega_{ii} - \omega_i)} = \frac{\omega_s B_{inj\_fii} - \omega_i \Delta B_s}{\omega_s(\omega_{ii} - \omega_i)}, \tag{90}$$

$$L_{CoilTot} = \frac{\omega_{ii} - \omega_i}{\omega_s}\frac{1}{\omega_i \Delta B_s - \omega_s B_{inj\_fi}} = \frac{\omega_{ii} - \omega_i}{\omega_s}\frac{1}{\omega_s B_{inj\_fii} - \omega_{ii}\Delta B_s}. \tag{91}$$

6.3.2 Indirect zero-sequence voltage measurement

All the measurement circuits are implemented in the device (EGE spol. s r.o, 2020, p. 2). MCI measures the voltage response of the network directly at the power auxiliary winding (PAW) where the current signal is injected (A. Eberle Gmbh & Co.KG, 2020, p. 1). The actual zero-sequence voltage response in the primary is then evaluated from the voltage on the PAW. To achieve this, a mathematical model of the ASC is used for each frequency component, allowing for the recalculation of the measured secondary voltage to its corresponding primary side voltage component (Vancata & Matuljak, 2019, p. 4).

The idea of indirect zero-sequence voltage measurement is to increase the accuracy of the measurement as it is claimed that the accuracy of the measuring winding of ASC is not high enough for the correct measuring of relatively low voltage value and phase shift (Vancata & Matuljak, 2019, p. 4). A further benefit is simplicity since no external measurements or installations are needed. However, the indirect voltage measurement must sufficiently accurately evaluate primary values. To improve results, the MCI is initially calibrated at the coil to account for all non-linear effects, as the ASC is a non-ideal transformer (A. Eberle Gmbh & Co.KG, 2020, p. 1). This ensures that the voltage measured through the PAW is not dependent on the position of the coil.

Komrska et al. (2018) derived a frequency-independent mathematical model of ASC, which enables recalculating quantities from the secondary to the primary side of the coil. To identify the mathematical model with constant parameters, independent of frequency, a series of measurements have been performed on the ASC (Komrska et al, 2018, pp. 4328–4330). This includes measurements with open and shorted primary windings.

7 Conclusion

Compensated distribution networks are increasingly adopted worldwide due to their advantages, notably the low earth fault current. The injection of an auxiliary zero-sequence current signal is a critical method providing solutions to various complex applications in compensated networks. These include tuning arc suppression coil, detecting high impedance faults, locating earth faults, and residual earth fault currents compensation. Addressing these challenges ensures the optimal performance and positive properties of compensated networks.

This thesis described the concept, implementation, and applications of current injection via power auxiliary winding of the arc suppression coil. The injection theory is further derived, including relevant equivalent circuits and equations describing the system's response to injection and the parameters affecting it. The injection theory was then verified and visualized using a PSCAD simulation model and MATLAB software.

According to the injection theory, the system's response to the fundamental frequency injection is primarily influenced by the magnitude and phase shift of the injected current, system unbalance, damping, and detuning. On the other hand, the magnitude and frequency of the injected current and the system damping and detuning primarily determine the system's response to the injection of frequencies unequal to the fundamental frequency. Moreover, it is shown that the resonant frequency of the systems depends on the ratio of the network inductive current to the capacitive current.

Finally, a comprehensive literature review was conducted on commercial injection-based coil tuning solutions, considering products from the leading vendors. The first injection solutions utilized a single frequency injection of 50 or 60 Hz current. However, due to the inherent disadvantages of fundamental frequency injection, more sophisticated methods were developed. Next-generation injection solutions then utilized the two most dominant side frequencies produced by pulsing a 50 Hz signal. The latest and most

innovative solution was ultimately introduced by the Multi-Frequency Current Injection (MCI) a few years ago.

The pioneering approach and design of the MCI produce a multifrequency signal consisting of eight distinct frequencies enabling precise coil tuning over the whole ASC tuning interval. Notably, the MCI also introduced the concept of utilizing complementary frequencies and implemented an indirect measurement of the zero-sequence voltage. These novel features have significantly enhanced the accuracy and effectiveness of coil tuning in compensated networks.

Future research could include a more comprehensive simulation model, incorporating multiple feeders with loads and line series impedances and a non-ideal arc suppression coil equipped with a non-ideal power auxiliary winding. Further research on the practical implementation of the current injection, including system measurements, would complement this thesis. Also, verifying the current injection theory in practice through field tests would be a remarkable progression. Finally, the theoretical background of other applications of current injection beyond arc suppression coil tuning could be reviewed and documented more thoroughly.

References

ABB. (2004). *Menetelmä kompensointikuristimen säätämiseksi sähkönjakeluverkossa*. (Finnish patent number FI 113592 B). Finnish patent and registration office. https://patentimages.storage.googleapis.com/c5/05/17/ae7cf68ee76051/FI113592B.pdf

ABB. (2023). *REX640 Technical Manual*. https://search.abb.com/library/Download.aspx?DocumentID=1MRS759142&LanguageCode=en&DocumentPartId=&Action=Launch

A. Eberle Gmbh & Co.KG. (2017). *Operating Instructions for The Petersen-Coil Regulator*. https://www.a-eberle.de/wp-content/uploads/2020/06/BA_REG-DPA_EN.pdf

A. Eberle Gmbh & Co.KG. (2020). *Multifrequency Current Injection MCI*. https://www.a-eberle.de/wp-content/uploads/2020/05/TD_MCI_EN.pdf

A. Eberle Gmbh & Co.KG. (2023). *Multi-Frequency Current Injection for Low or Highly Variable Zero-Sequence Voltages MCI*. https://www.a-eberle.de/en/products/mci-multi-frequency-current-injection-for-low-or-highly-variable-zero-sequence-voltages/#undefined

Buigues, G., Valverde, V., Zamora, I., Mazón, J., & Torres, E. (2012). *Signal injection techniques for fault location in distribution networks*. In International Conference on Renewable Energies and Power Quality (pp. 412–417). https://doi.org/10.24084/repqj10.330

Druml, G., & Papp, K. (1996). *Unipolar earth leakage recognition process for three phase mains* (International publication no. WO/1996/027138). https://patentscope.wipo.int/search/en/detail.jsf?docId=WO1996027138&_cid=P11-LJ1CU8-71201-1

Druml, G., Kugi, A., & Parr, B. (2001). *Control of Petersen coils*. In XI. International Symposium on Theoretical Electrical Engineering. https://www.hvpower.co.nz/TechnicalLibrary/RE+DS/Control%20of%20Petersen%20coils.pdf

Druml, G., & Kugi, A. (2005). *Determining parameters of Petersen-coil compensated network without de-tuning the coils, by feeding composite current into zero-phase system, and measuring voltages* (German publication no. DE10307668B3). https://patents.google.com/patent/DE10307668B3/en

Druml, G., Kugi, A., & Seifert, O. (2005). *New method to control Petersen coils by injection of two frequencies*. In *CIRED 2005-18th International Conference and Exhibition on Electricity Distribution* (pp. 1-5). IET. http://www.cired.net/publications/cired2005/papers/cired2005_0399.pdf

Druml, G., & Seifert, O. (2005). *New Method for the State Evaluation of the Zero-Sequence System*. https://citeseerx.ist.psu.edu/document?repid=rep1&type=pdf&doi=9d551d17899594149aff16cbffddaa9f6f762292

Druml, G., & Kugi, A. (2007). *Method for detecting and locating low-resistance and high-impedance ground faults in electrical supply networks* (German publication no. DE10307972B4). https://patents.google.com/patent/DE10307972B4/en

Druml, G., Steger, S., Seifert, O., & Kugi, A. (2007). *Operational experiences with the new method to control petersen coils by injection of two frequencies*. In Proceedings of 19th International Conference on Electricity Distribution (pp. 1-4). http://www.cired.net/publications/cired2007/pdfs/CIRED2007_0089_paper.pdf

Druml, G., Raunig, C., Schegner, P., & Fickert, L. (2012). *Earth fault localization with the help of the fast-pulse-detection-method using the new high-power-current-injection (HPCI)*. In 2012 Electric Power Quality and Supply Reliability (pp. 1-5). IEEE. https://doi.org/10.1109/PQ.2012.6256231

Druml, G., Raunig, C., Schegner, P., & Fickert, L. (2013). *Fast selective earth fault localization using the new fast pulse detection method*. In 22nd International Conference and Exhibition on Electricity Distribution (CIRED 2013) (pp. 1-5). IET. https://doi.org/10.1049/cp.2013.1068

EGE spol. s r.o. (2020). *MCI P-01 Multifrequency current injection datasheet*. https://www.ege.cz/en/products-and-services/electrical-engineering-division?bsgrid-col12983-id=11169&do=bsgrid-col12983-download

Farughian, A., Poluektov, A., Pinomaa, A., Ahola, J., Kosonen, A., Kumpulainen, L., & Kauhaniemi, K. (2018). *Power line signalling based earth fault location*. The Journal of Engineering, 2018(15), 1155-1159. https://doi.org/10.1049/joe.2018.0190

Habib, M. Z. (2022). *Fault location in resonant earthed medium voltage distribution systems* [Doctoral dissertation, KTH Royal Institute of Technology]. http://urn.fi/urn:nbn:se:kth:diva-321739

Hänninen, S. (2001). *Single phase earth faults in high impedance grounded networks: characteristics, indication and location* [Doctoral dissertation, Helsinki University of Technology]. VTT Technical Research Centre of Finland. ISBN 951-38-5961-4. https://aaltodoc.aalto.fi/handle/123456789/2212

Janssen, M., Kraemer, S., Schmidt, R., & Winter, K. (2003). *Residual current compensation (RCC) for resonant grounded transmission systems using high performance voltage source inverter*. In 2003 IEEE PES transmission and distribution conference and exposition (IEEE Cat. No. 03CH37495) (Vol. 2, pp. 574-578). IEEE. https://doi.org/10.1109/TDC.2003.1335338

Komrska, T., Talla, J., Košan, T., & Peroutka, Z. (2018). *Identification of Mathematical Model of Arc Suppression Coil*. In IECON 2018-44th Annual Conference of the IEEE Industrial Electronics Society (pp. 4327-4331). IEEE. https://doi.org/10.1109/IECON.2018.8592784

Lakervi, E., & Holmes, E. (1995). *Electricity Distribution Network Design* (2nd edition). The Institution of Engineering and Technology. ISBN 0-86341-309-9

Lakervi, E., & Partanen, J. (2009). *Sähkönjakelutekniikka* (2nd edition). Gaudeamus Helsinki University Press. ISBN 978-951-672-359-7

Levashov, V., Winter, N., & Winter, A. (2021). *Ultra-sensitive localization and neutralization of low and high impedance earth faults in distribution networks*. In CIRED 2021-The 26th International Conference and Exhibition on Electricity Distribution (Vol. 2021, pp. 1111-1115). IET. https://doi.org/10.1049/icp.2021.1817

Matuljak, I., & Vancata, P. (2016). *Method and device for automatic tuning a continuously and/or discretely tunable arc suppression coil in the compensated network of an electrical system* (International publication no. WO/2016/029890). Patentcentrum sedlan & partners S.R.O. https://patentscope.wipo.int/search/en/detail.jsf?docId=WO2016029890

Mäkinen, O. *Sähköverkot*. J. Koski, *SATEC2190: Sähköverkot*. Vaasa university of applied sciences.

Raunig, C., Fickert, L., Obkircher, C., & Achleitner, G. (2010). *Mobile earth fault localization by tracing current injection*. In Proceedings of the 2010 Electric Power Quality and Supply Reliability Conference (pp. 243-246). IEEE. https://doi.org/10.1109/PQ.2010.5549991

Schiner, T., & Schlömmer, M. (2022). *Advanced Residual Current Compensation System*. In 2022 IEEE/PES Transmission and Distribution Conference and Exposition (T&D) (pp. 1-5). IEEE. https://doi.org/10.1109/TD43745.2022.9817003

Schlömmer, M., Schinerl, T., & Osterkorn, H. (2017). *Impact of voltage fluctuation on Petersen-coil control and results of a tuning method with evaluation of side frequencies*. In 24th international conference on electricity distribution (pp. 12-15). http://cired.net/publications/cired2017/pdfs/CIRED2017_0170_final.pdf

Sheta, A. N., Abdulsalam, G. M., & Eladl, A. A. (2020). *A Survey of Fault Location Techniques for Distribution Networks*. (Dept. E). MEJ. Mansoura Engineering Journal, 45(2), PP 12-22. https://doi.org/10.21608/bfemu.2020.98825

Talla, J., Blahnik, V., & Kosan, T. (2016). *Grid impedance identification by current harmonics signal injection*. In 2016 ELEKTRO (pp. 387-390). IEEE. https://doi.org/10.1109/ELEKTRO.2016.7512103

Tengg, C., Schoass, K., Druml, G., Schmaranz, R., Marketz, M., & Fickert, L. (2013). *Evaluation of new earth fault localization methods by earth fault experiments*. In 22nd International Conference and Exhibition on Electricity Distribution (CIRED 2013), Stockholm, (pp. 1-4). https://doi.org/10.1049/cp.2013.1179

Trench Austria GmbH. (2003). *Neutral Point Treatment - Technical Product Presentation*. https://docplayer.net/51679154-Trench-austria-neutral-point-treatment-technical-product-presentation.html

Trench Group. *Earth-Fault Compensation Controller EFC60m*. https://www.maviko.fi/wp-content/uploads/2020/01/EFC60m_esite_eng.pdf

Trench Group. (2013). *Earth-Fault Compensation Controller EFC50 / EFC50i*. https://docplayer.net/5795917-Earth-fault-compensation-controller-efc50-efc50i-the-proven-power.html

Trench Group. (2021a). *Earth-Fault Compensation Controller EFC60m*. https://trench-group.com/wp-content/uploads/2021/03/EC60m_Eng.pdf

Trench Group. (2021b). *Earth-Fault Compensation Controller EFC60s*. https://trench-group.com/wp-content/uploads/2021/03/EFC60s_Eng.pdf

Vancata, P., & Matuljak, I. (2019). *New method of arc suppression coil tuning using truly multifrequency current signal*. In CIRED 2019-The 25th International Conference and Exhibition on Electricity Distribution. http://dx.doi.org/10.34890/23

Vancata, P., Matuljak, I., & Tomas, X. (2021). *Practical use of a new method of arc* suppression *coil tuning*. In CIRED 2021-The 26th International Conference and Exhibition on Electricity Distribution (Vol. 2021, pp. 1217-1221). IET. http://doi.org/10.1049/icp.2021.1990

Wahlroos, A., Altonen, J., & Automation-Finland, A. O. D. (2011). *Compensated networks and admittance based earth-fault protection*. In Kaunas University of Technology and Aalto University organized seminar on Methods and techniques for earth fault detection, indication and location, Espoo, Finland. https://search.abb.com/library/Download.aspx?DocumentID=1MRS757370

Wahlroos. (2017). *Maasulkusuojauksen uudet haasteet ja suojausalgoritmien kehitys*. K. Kauhaniemi, SATE3160: *Sähköjärjestelmien suojaus*. University of Vaasa.

Wahlroos, A., Altonen, J., & Xavier, J. (2021). *Can compensated networks be an alternate solution to reduce the risk of ground faults causing forest fires?*. In 2021 74th Conference for Protective Relay Engineers (CPRE) (pp. 1-34). IEEE. https://doi.org/10.1109/CPRE48231.2021.9429843

Wahlroos, A. (2023). *Kompensoitu verkko ja maasulkusuojaus*. Relesuojauksen jatkokurssi sähkölaitoksille.

Wang, W., Yan, L., Fan, B., & Zeng, X. (2016). *Control method of an arc suppression device based on single-phase inverter*. In 2016 International Symposium on Power Electronics, Electrical Drives, Automation and Motion (SPEEDAM) (pp. 929-934). IEEE. https://doi.org/10.1109/SPEEDAM.2016.7526025

Yang, H., Tang, J., Hou, H., Wu, X., & Bian, X. (2019). *A novel zero-residual-current arc suppression method using single-phase voltage source inverter*. In 2019 IEEE Innovative Smart Grid Technologies-Asia (ISGT Asia) (pp. 2042-2046). IEEE. https://doi.org/10.1109/ISGT-Asia.2019.8881687

Yu, K., Yu, Q., Zeng, X., Zeng, J., Ni, Y., Zou, H., & Liu, F. (2022). *A novel method of high impedance fault detection and fault resistance calculation based on damping rate double-ended measurement for distribution network*. International Journal of Electrical Power & Energy Systems, 136, 107686. https://doi.org/10.1016/j.ijepes.2021.107686